An International Forum For The AE Science and Technology

JOURNAL OF ACOUSTIC EMISSION

Vol.30/January-December 2012

EWGAE30 - ICAE7
Granada, Spain

Endorsed by AEWG and EWGAE

Published by
Acoustic Emission Group
Encino, CA USA

Journal of Acoustic Emission, Volume 30, 2012

CONTENTS

30-180 Research and Applications of AE on Advanced Composites
Kanji Ono and Antolino Gallego

* indicates the availability in CD-ROM only. Indices are also available for download from www.aewg.org.

Meeting Calendar

AEWG 55

The 55th Meeting on Acoustic Emission Working Group will be held on June 11-12, 2013 at Garden Grove, CA. The host is Dr. Jerry Huang of Boeing (jerry.q.huang@boeing.com). More information is available at www.aewg.org. For accommodation, contact Crowne Plaza Anaheim Resort at http://www.anaheim.crowneplaza.com/

AE Activity

EWGAE30-International Conf. on AE 7, 2012

Information on this successful conference is available at www.ewgae.es, including Program and Proceedings in downloadable pdf file. See also a report on the conference at http://www.ndt.net/search/docs.php3?id=13636&content=1

Announcement

With the publication of this volume, this Journal will shift to the open-access mode, terminating the paper/CD distribution and subscription services. I wish to thank all of you, authors, reviewers, co-editors, book agencies and readers, who have supported this Journal for the past 32 years. Some of the reasons for the founding of this publication have faded as there are so many venues for quality publications. In particular, academic authors require impact factors, which are incompatible with our goals. We will continue providing a forum in timely manner with web-based distribution, rather than annual basis, with rigorous review as in the past to maintain the quality we have sustained. We hope future contributors and readers keep the confidence in Journal of Acoustic Emission in the new approach for disseminating the information useful to the global AE community.

Kanji Ono, Editor and Publisher

Research and Applications of AE on Advanced Composites

Kanji Ono[1] and Antolino Gallego[2]
[1] Department of Materials Science and Engineering, University of California, Los Angeles, CA 90095, USA
[2] University of Granada, 18071 Granada, Spain

Abstract

This paper reviews progress in acoustic emission (AE) research and its applications to high performance composite materials and structures. The achievement and inadequacy in understanding of AE from composites are examined along with cases of successful usage in commercial and aerospace fields, taking into account limitations due to high attenuation and anisotropy. New goals for the future are also discussed in view of new analytical tools and vastly advanced instrumentation.

Keywords: attenuation, localization of damage, inspection, Lamb waves, wave propagation, finite element method (FEM), frequency analysis, modeling and simulation, pattern recognition, signal processing, aerospace, chemical and petrochemical, advanced composites, fiber reinforced materials, pressure vessel, structural health monitoring, composite structural evaluation, composite materials NDT.

1. Introduction

Acoustic emission (AE) played an important role in the development of glass-fiber reinforced composite (GFRP) rocket motor cases for Polaris A3 circa 1962 [1]. It was the beginning of AE applications that have expanded greatly over the last 50 years. AE was next deployed in testing propellant tanks for the Apollo lunar module and other aerospace applications [2]. Aerojet engineers recognized the variation in AE to originate from resin, interlaminar and fiber failures [1, 2] and modified manufacturing processes, e.g., by eliminating the geometrical inflection points in design to reduce the interlaminar shear stresses [3]. They used the summation of AE amplitude to successfully predict the burst pressure and developed practical AE source location equipment [1]. Continued work on rocket motor cases at Thiokol introduced Kaiser effect and load-hold emissions to the burst pressure prediction [4]. These pioneering accomplishments still form the backbone of AE pressure vessel inspection technology today.

Research on fiber-reinforced composites started in early 1970s [5-7]. Results verified correlations of AE to micro-fracture mechanisms. In one of the earliest AE papers on composite materials research, Liptai [5] showed the breakdown of Kaiser effect (this is now known as Felicity effect) and gradual reduction of Felicity ratio (aka Load ratio per JSNDI for concrete applications) in cyclically loaded fiberglass reinforced plastic (FRP) NOL rings. The latter was recognized as static fatigue (or stress rupture, a well-known glass failure mode due to load hold) of glass fibers, but no follow-up AE study was apparently published. Significance of these findings was initially unnoticed, however. Kim et al. [6a] clearly observed Felicity effect in carbon fiber reinforced plastic (CFRP) as well, but dismissed this effect while Kimpara [6b] also found Felicity effect, but treated it as error. The first peer-reviewed paper on composite research seems to be from UCLA's Tetelman group on boron-epoxy composite [7]. They correlated fiber fracture to AE, electrical resistance and compliance changes.

A breakthrough came in 1977 when Fowler recognized that AE activities found before reaching prior maximum load indicate the degradation of FRPs [8, 9]; for this behavior, he coined a new term, Felicity effect, and defined Felicity ratio as (load at AE re-start during reloading)/(prior maximum load)[see also the follow–up work, 10-12]. Subsequently, the Committee on Acoustic Emission from Reinforced Plastics (CARP) was organized, including Fowler, Teti, Crump, Hagemeier among others [13, 14]. Through extensive collaborative field tests, CARP developed FRP inspection technology and published method documents through Society of the Plastics Industry, then through ASME/ASTM [15, 16]. This Recommended Practice spelled out loading scheme, AE analysis and interpretation methods and evaluation guideline, enabling widespread AE applications of FRP vessel examination, in chemical industry in particular. Fowler [12] documented success achieved in reducing major accidents via this AE method. In a revised document published in 1995 [17], intensity analysis method is used, relying on severity and historic index, along with emission during load hold, total counts, high amplitude emission, Felicity effect as key elements of evaluation. Dr. Fowler states (e-mail, 2012) "In the absence of CARP, the revised procedure became an open document. A number of organizations modified it for their own in-house needs. Some equipment vendors programmed it for use with their proprietary equipment. Even though not a public document, the technique has widespread use." His students extended its uses in FRP design and analysis [18, 19]. Fowler [20] and Davies [21] gave details of the intensity analysis method, which has also been used in MONPAC system for examining metal chemical processing equipment [22].

With improved FRP technology combined with the advances in AE instrumentation, numerous studies on research and applications followed and have been documented in AE Testing volumes of ASNT Nondestructive Testing Handbooks [23], where one can find many AE uses, such as for testing bucket-truck FRP booms. Also available are six-volume conference proceedings of AECM [24a-f], ASTM and ASME codes and standards, and many journal/conference articles that reach into thousands. Hamstad contributed important reviews [25, 26] along with his many papers with his extensive composite research since early 1970s. See also other notable reviews [12, 20, 27, 28]. Gorman [29] and Wevers [30] reviewed AE methods for structural health monitoring (SHM) field. See [31] for a review of newer AE analysis techniques. Drouillard and Hamstad indexed early AE papers in [32].

We must realize first that AE has not provided an effective NDT tool for some parts of composite industry. Such a tool is sensitive to existing defects, and is globally applicable to a large component in real time monitoring condition. While many success stories exist in FRP industry, as noted above by Dr. Fowler, AE has only played limited roles in many aerospace sites. We know AE can do better. In this paper, selected aspects of research and applications will be reviewed to highlight the progress achieved and to point to areas in need of more work. The main focus will be on development from the last 10-15 years since references cited above [23-30] have provided adequate coverage for the earlier period. Hopefully, we can go to the next level of understanding to give better solutions. Applications of advanced composites are expanding beyond aerospace and chemical industries into transportation industry and utilities. Such expansion presents renewed challenges for AE to be a worthy NDT method. We do have to overcome problems due to high signal attenuation in composites and need to explore the causes of Felicity effect and stress rupture, just listing a few. Collectively, we should resolve these obstacles, and make AE into a truly indispensable NDT method.

Research

Fiber fracture

From the early days of AE, glass fiber (GF) fracture has been recognized as energetic AE source detected close to the fracture load. AE from single fibers, tows (or strand) and unidirectional (UD) composites was initially characterized with amplitude distribution in order to compare with other failure mechanisms. By now, the difficulty of using AE amplitude by itself in signal discrimination is well recognized. However, a misconception that fiber fracture always produces high-energy event still persists to this day and this section is intended to clarify the situation.

For typical 10-μm diameter UD GFRP, peak amplitude ranges from 60-80 dB (ref. 1 μV=0 dB; literature in the 80s often used 1 μV=20 dB and one needs to reduce amplitude values by 20 dB) [33-35]. This range depends on the fiber diameters and sensors used, but GF results are fairly consistent over the years when sensor difference is accounted for. Wolters [33] used sensitive resonant sensors with less than 10-mm propagation distance and found 40-60 dB for 6 μm, 65-85 dB for 13 μm and 80-100 dB for 24 μm fibers, while another reported 50-70 dB for 13.5 μm GF [34]. In our test of woven GFRP [36], high amplitude AE signals of 60 dB mean level were found at above 90% of the failure load, verified as fiber fracture microscopically. Woven GFRP failure mechanisms are the subject of a detailed study [37], and complementary AE study should allow better understanding of woven composites, which are increasingly used in aircraft fuselage with carbon fibers, such as Boeing 787 (A.K. Mal, July 2012, private communication). Recent studies [38-40] reexamined single fiber composite (or SFC, with epoxy matrix) tests. Nordstrom [38] used 18-μm glass fibers and found peak amplitude of fiber fracture at 80 dB (150 kHz sensor). He also obtained Weibull moduli of 7-9 and correlated the shape of stress-strain curves to progressing fiber fracture (see also [41]). Bohse [39] used 20-μm glass fibers with peak amplitude of fiber fracture to be 58-81 dB (PAC-WD sensor used). More recently, de Oliveira [40] conducted careful SFC tests determining the amplitude of fiber breaks along with source location data. Such amplitude correction with source location was introduced earlier [42], but has seldom been used since. Carey [43] also introduced distance correction in his AE signature analysis work on CFRP. Using 21-μm GF, SFC showed 20-dB attenuation over 45 mm and fiber-break AE mean amplitude of 73 (53-79) dB (58 dB for 11-μm GF); the lower values are due to the use of a wideband sensor (DWC B1025). In single tow 9-μm GF composite experiment, Nanjyo et al. [44] obtained lower amplitude values ranging from 46-56 dB (Pico sensor). Diameter and sensor differences are responsible for the observed variation in amplitude ranges since GF strength and modulus are essentially unchanged. Berthelot obtained comparable amplitude range for 13-15 μm GF and for 7-μm T300 CF [45, 46].

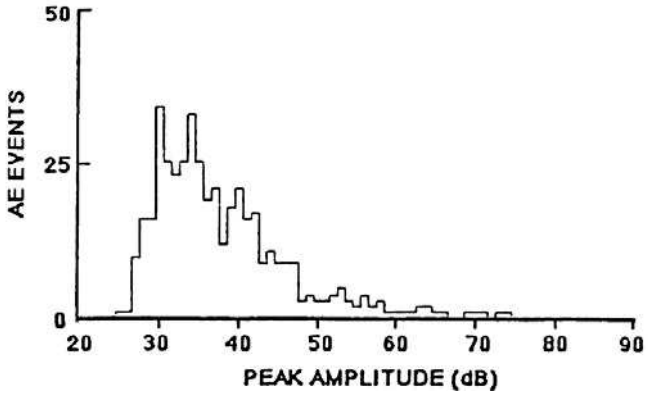

Fig. 1 Peak amplitude distribution of fiber fracture at 40-60% of the fracture load from 9-ply UD sample with pre-cut mid-plies [48]. Celion G50 fiber.

When carbon fibers (CF) were tested initially, peak amplitude of AE signals for T300 CF was 30 dB less than glass fiber [34, 47]. In part, this is because most carbon fibers have 7-μm diameter, and earlier CF strength was lower (T300 tensile strength = 2.65 GPa circa 1982). In our study [48, 49], the peak amplitude range was 30-50 dB for Celion G50 UD composites of various cut-ply arrangements (MAC175 sensor). This is 10+ dB lower than our GF results [36]. These AE signals from CF started to occur at 25-33% of the composite strength and also had short duration (mostly <50 μs) [34, 47, 48]. Figure 1 shows the peak amplitude distribution due to fiber fracture at 350-530 MPa, corresponding to 40-60% of the fracture stress from 9-ply UD sample with the middle 3 plies pre-cut [48]. Berthelot [46, 75] and Awerbuch [50] observed similar amplitude range (30-50 dB) during tensile and fatigue tests of CFRP coupons (CF not specified in [50], but probably T-300). Nanjyo's tow composite tests in 1992 [44] were also conducted for PAN (M50, 5-μm diameter) and pitch (XN50, 10 μm diameter) CF as well, giving comparable amplitude as GF data cited above; 44-56 dB for M50 and 38-58 dB for XN50. These CF were stronger than T300 or G50; 4.2 GPa for M50 and 3.7 GPa for XN50, accounting for the higher amplitude by nearly 20 dB (Fig. 2). In this study [44], the Weibull analysis of CF fracture strength and AE hits-strength distributions was reported. For three lots of CF, Weibull moduli of 5.7 to 13 were found for the fracture strength, while AE hits had higher Weibull moduli, m = 7 to 35, indicating multiple CF fracture in the tow tests [44]. A recent statistical analysis of AE signals from non-bonded GF bundles showed m to be 2.8-4.0 for 15-μm diameter fibers [41], which are about a half of m = 5.6 to 9 in tow tests [38, 40].

Recently, a new method for composite fracture study appeared [51, 52]; this is "High resolution Synchrotron Radiation Computed Tomography (SRCT)" and was used to capture fiber damage progression in a cross-ply CFRP laminate. Wright [51] showed that transverse-ply cracks initiate at 20% of the failure load, whilst 0º-splitting initiates at ~40% and large delaminations at ~60%. It is important to note that these cracking events occur in advance of significant fiber breaks that start after 60%. In Scott [52], fiber fracture was analyzed and compared with other studies, including AE. AE results for fiber fracture accumulation showed the same trend as SRCT and Weibull moduli are similar (also similar to [38, 40, 44]). The number of fiber breaks (N_f) was found to follow

$$N_f = C\,(\sigma/\sigma_o)^m, \qquad (1)$$

where σ is stress and σ_o is characteristic stress and m is Weibull modulus. See also [38]. It is hoped this method can be used widely leading to more definitive AE mechanistic studies.

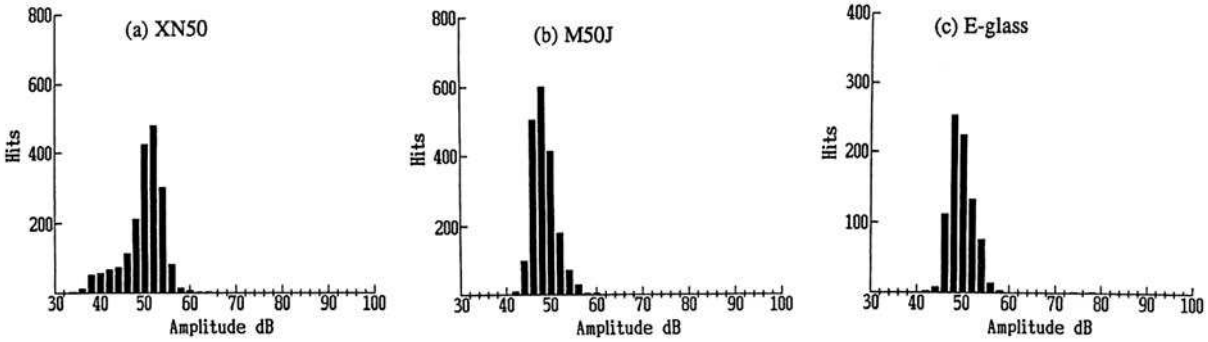

Fig. 2 Peak amplitude distribution of fiber fracture of a) XN50 pitch CF, b) M50 PAN CF, c) E-glass fiber tow-composite samples. Pico sensor. [44]

SFC tests with 7-μm carbon fibers, Bohse [39] showed amplitude of fiber fracture at 45-75 dB with the median value of 65 dB (WD sensor used; fiber unidentified, but ~late-90s vintage), comparable to usual GF fracture amplitude. In this work, CF diameter is ~1/3 of GF (–18 dB in

area) and less than 10 dB amplitude difference implies that higher CF modulus (by a factor of 3.5) accounted for the comparatively stronger AE in CF fracture (assuming comparable fracture strains). This CF SFC fracture result is 20-30 dB higher than previous studies from the 1980s [34]. This higher range of AE amplitude for CF fracture seems to reflect higher CF strength (2.5 GPa for G50 to 6.3 GPa for Toray T1000) and higher fracture strain values (0.7% for G50 to 2.2% for T1000). This is obviously due to dramatic improvements of CF properties in the last three decades. Thus, if one uses newer CF fracturing at 3-5 GPa (50-80% of T1000 fiber strength) in lieu of the G50 CF fractured at 350-530 MPa in 1988, 40 dB stronger AE signals are expected. Thus, we should observe CF fracture amplitude of similar or higher magnitude as 10-µm GF. In fact, Sause et al. [53] showed this recently. Comparing E-GF (6.5 µm) and T800-CF (5.2 µm), he obtained fiber fracture energy of 12.6 and 13.1 mNm^3/s^2. Assuming similar signal durations, the amplitude is expected to be comparable for comparable fiber diameters. It should be clear that AE amplitude from fiber fracture can vary widely. Small diameter, low strength CF produces AE amplitude comparable to the matrix sources (in 30-40 dB), while larger diameter fibers lead to higher amplitude to 80 dB. For thicker filaments, it can be even higher; AE signals from 150-µm boron filaments produced 95+ dB signals [54]. Fiber optic samples also give similar strong AE.

Recent tow composite tests using T1000 CF indicates the number of CF fracture at stresses below 60% of the fracture strength is grossly reduced with improved CF quality (no amplitude data was reported unfortunately) [55]. Figure 3 shows this behavior in tensile testing with intermittent load hold (ILH) for characterizing Felicity ratio, but cumulative hits start to rise rapidly after the fifth load hold or at 213 lbs (failed at 352 lbs) or 60.5% of 6.77 GPa fracture strength. The same NASA group examined Kevlar tow composites as well. In this case, fibers start to fail at ~90% of the fracture strength [56]. This behavior is in common with GF composites. Detailed analysis of these experiments of UD composites should clarify this situation on amplitude levels.

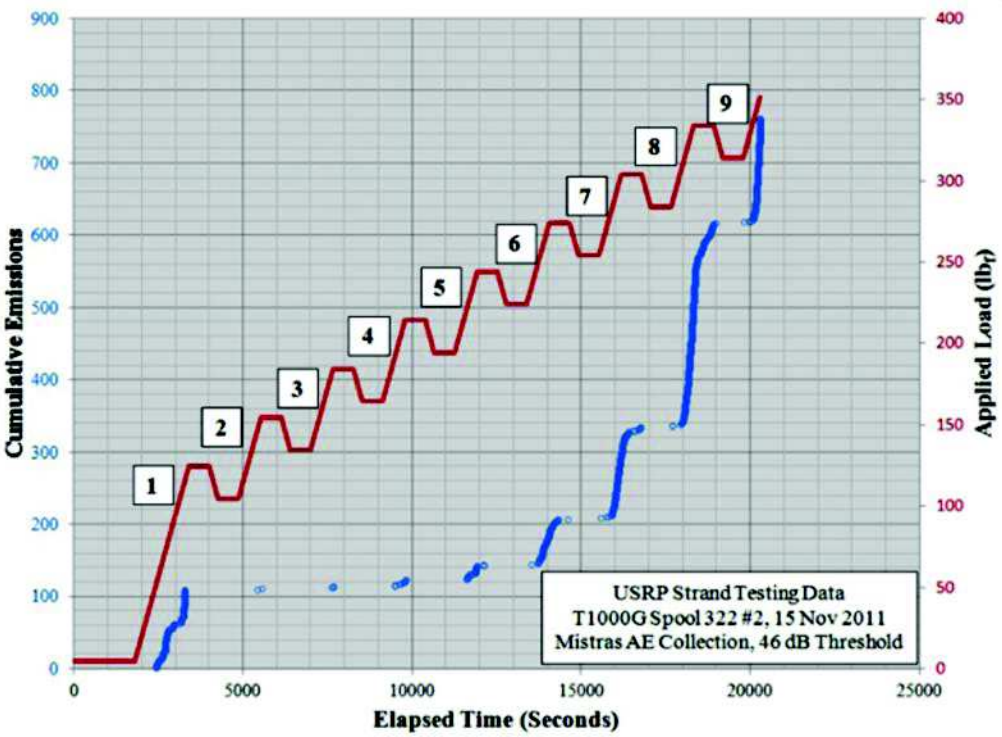

Fig. 3 AE of T1000 CF tow-composite test using ILH schedule at NASA. Red: Applied load (in lbs), Blue: AE. [55] (1 lbs = 4.54 N)

When a carbon or glass fiber fractures, it does so in brittle manner. Typical crack velocity in brittle fracture is several tenths of mm/μs or higher (e.g., 0.52 mm/μs for PMMA [57] and 1.6 mm/μs for glass [58]). Actual cracking velocity is expected to be much smaller as a static crack needs to accelerate under stress. For GF and CF, fracture time is expected to be 0.7~2 μs assuming crack velocity of 5~10 m/s (or μm/μs). The lower velocity limit is for GF [58], while CF crack velocity is expected to be twice that since CF moduli are ~4 times that of GF (crack velocity scaling with the Rayleigh velocity [57]). This translates to the center frequency of 0.5~1.4 MHz for AE signals from fiber fracture, which is partially within the high frequency range of common AE sensors, such as PAC WD, Pico and DWC B1025/B1080. Indeed, Gorman [59] reported such fiber-break signals from a COPV cover the entire range of flat sensor response (20-400 kHz), in contrast to matrix cracks (splitting), for which detected signals had frequency contents confined below 50 kHz. He also observed that, in hundreds of pressure vessel tests, including both CFRP and FRP vessels, waves with the highest frequencies appeared when the load or pressure level exceeds above 80% of ultimate stress. Thus, tow composite behavior extends to the windings of COPV. SFC samples in de Oliveira's study also showed high-frequency components [40]. His signals contained strong 300-1050 kHz components (using DWC B1025), especially when debonding accompanies a fiber break or when 7-μm CF SFC has a fiber break. He attributes the effect of debonding to the higher freedom of the fiber ends at fracture. In contrast, GF fiber break signals without simultaneous debonding (11 and 21 μm GF) have the highest peak at ~170 kHz with gradually decreasing high-frequency components. Gorman [59] observed similar vibration-induced AE from broken ends of tows and further clarification of debonding may be worthwhile in providing new inspection scheme. It should be noted here that Kim and Nairn [60] showed that fiber-matrix debonding always accompanies a fiber fracture in GF and CF SFC. Their epoxy resin (Epon 828) did not exhibit flat or conical fracture envisioned by earlier work [34]. We must have independent proof before assigning to an AE cluster a mechanism of fiber fracture with or without debonding.

When using broadband sensors, the observed peaks in the frequency spectra have to be treated with caution. Unless one has broadband flat-in-frequency sensor and propagation path, the peak frequency differs from the source-defined frequency. Most available sensors today have limited frequency range and have resonance peaks. Sheet or plate geometry has preferential frequency ranges of wave propagation. For example, Bohse [39] correlated fiber fracture to 500-kHz peak using WD sensor while matrix fracture contains lower frequency peaks only. This work and many others clearly demonstrated that one can often identify AE mechanisms via the frequency domain information. In fact, it is an important part of our pattern recognition analysis studies on composite AE [61a-c]. On the other hand, one cannot conclude fiber fracture has such a frequency peak because the WD sensor used is the origin of this peak (WD has three main resonances including one at 500 kHz [62]). Such arguments assigning frequency peaks to some specific AE sources have shown up too often in the past [63-65], yet most such claims revert to specific sensor or sample resonances and sensor-source path has significant effects. For example, de Groot et al. [64] examined a variety of CFRP and assigned frequency ranges to specific mechanisms. Such correlation is valid for the test condition they utilized, but the particular peaks originated from the use of WD sensor again, which was also the sensor used in Giordano et al. [65]. Eaton et al. [66] warned that "the overriding effects of specimen geometry and sensor response can produce misleading results" in their study to use frequency for separating source mechanisms having the differing relaxation time. One should not expect specific frequency peaks in other test arrangements, except for the general concept of faster source events to have higher frequency contents. It is instructive to refer to the most broadband AE study reported to date by Scruby and Battle, extending the limit to 3 MHz (–6 dB point) [67]. They did find two peaks for

the signal from fatigue crack propagation, the main one at 600 kHz. However, these peaks are due to the normal modes of the sample. Even more broadband system is needed to identify the key frequency of fiber fracture via the frequency spectrum analysis since fracture time is quite short, on the order of 0.1-1 μs.

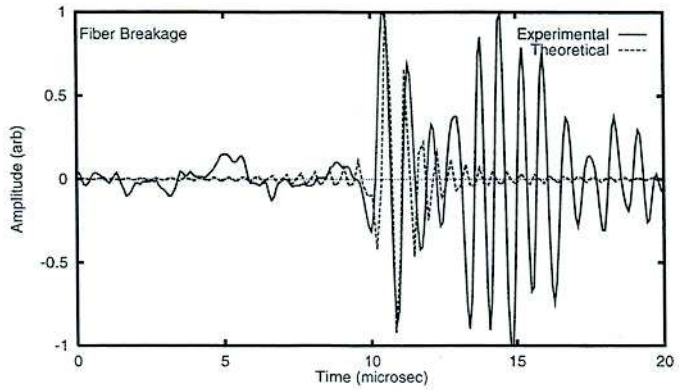

Fig. 4 Waveforms of fiber fracture (theory-broken line; experiment-solid line). [68]

This situation regarding the frequency peaks also arises in theoretical studies. For example, Guo et al. [68] obtained the solution of the wave motion produced by a general source in a composite plate using laminate theory with transverse shear correction. He identified the distinguishing features of the wave motion produced by various micro-fracture events (e.g., matrix cracking, delamination, fiber break, etc.) in thin composite laminates. Guo represented fiber fracture with 0.125-μs cracking time in a model CFRP plate among others. Using the experimental transfer function of a broadband sensor (B1025) showing 200-2000 kHz bandwidth (within 3 dB of the peak at 1 MHz,), the calculated waveform for CF fracture shows dominant ~1 MHz oscillations. See Fig. 4. The apparent frequency in this waveform is much lower than the expected center frequency of the original crack model, or 8 MHz. Note that Guo did not claim fiber fracture AE to have 1 MHz peak frequency. Recently, Sause [69] used finite-element modeling of laminated composites and crack models for CF fracture (in-plane) and resin fracture (out-of-plane) with 0.1-μs cracking time. The CF crack produced displacement signals dominated by ~1-MHz S_o waves (where So velocity starts to decrease sharply), whereas the resin crack produced 100-300 kHz A_o waves. His model included Lamb wave propagation of 50 mm from the source. Here, the Lamb-wave dispersion effects play the central role in limiting the upper frequency limit of the simulated AE signal and deciding the centroid frequency. Sause has presented more extensive analysis of related modeling in his thesis work [70]. His results point to the additional factor we must consider in trying to assess the source function when AE moves through thin sheets/plates. [It is noted that Ichikawa et al. [A1] reported theoretical calculations for the intensity of Lamb wave modes and dispersion effects as a function of frequency-thickness product. They used steel as the medium, but confirmed the Lamb-wave behavior observed by others. See Appendix 1.]

In considering the frequency contents of AE signals, one must not forget that high frequency components are attenuated rapidly as the signals travel from the source to sensors. Unless the sensors are almost over the source, the high frequency components above 200-300 kHz are reduced to background beyond 0.5~1 m distance. This has been known for 30 years and was incorporated in the CARP procedures, but we have no effective remedy applicable to typical applications. In laboratory, sensors are close to sources and we can try to understand the basic behavior.

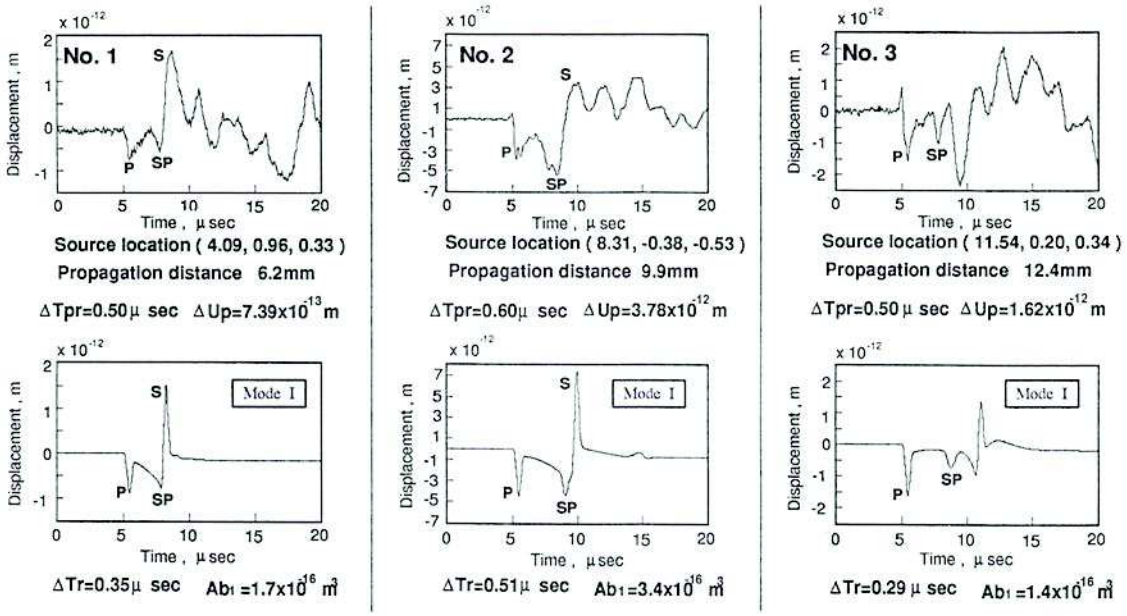

Fig. 5 Observed and matched calculated waveforms with source parameters. UD GFRP test. [71]

Another approach to the study of fiber-AE originated from Takemoto group at Aoyama Gakuin University. Suzuki et al. [71] conducted elaborate experimental analysis of GF fracture, deducing the source function for detected AE signals during tensile testing of UD FRP. The goal of getting the force-time function of an AE source is similar to the deconvolution approach from the 1980s, but waveform simulation and matching of source parameters distinguish this method from the past attempts [72]. Suzuki [71] incorporated the viscoelastic nature of FRP by introducing a frequency independent relaxation function, R(t), after Weaver [73] and extended the Green's function approach of Ohtsu and Ono [74]. Suzuki [71] used a NIST-type displacement sensor, as well as an 8-channel source location system that identified the source position (using 8 Pico sensors). Both displacement waveform and location data were fed as input to waveform simulation algorithm. Adjusting the source rise time and crack volume, theoretical and experimental waveforms were matched. Here, the latter waveform was obtained by a conical displacement sensor of NIST design derivative (PAC S9208). Examples of such pair are shown in Fig. 5 for fiber-break cases. A cross plot of source parameters, crack volume vs. rise time, in Fig. 6, indicates the crack velocity limits of 2-22 m/s. The median crack velocity is 6.5 m/s in a good agreement with the measured crack velocity in glass of 5 m/s [58].

Note that, in elastodynamic theory [73, 74], the source parameter representing its magnitude is given by the product of the source area (A) and displacement (b_i), or crack volume. In fiber fracture, fiber opening equals b_i, not the released elastic energy. Thus, the energy analysis given in the past, such as by Lorenzo [70] and Berthelot [75] needs to be modified. Another overlooked aspect of AE signal analysis is the modeling of sensor input. For example, Berthelot [75] used a rectangular pulse to represent a crack signal, which is a sensible first-order approximation for surface displacement due to an opening crack detected at the epicenter. Note that the source displacement function is step-wise, but with a slope (Fig. 4 in [75]). Because Green's function is convolved with the source [74], surface displacement becomes a Gaussian-type mono-pole pulse (left: Fig. 5, [75]). It was simplified to a rectangular one (right: Fig. 5, [75]). AE sensors, however, typically respond to the velocity component. Thus, the sensor responds to two sharp pulses of opposite polarity separated by the duration of the rectangular pulse (T_f). In this case, the FFT of the velocity response has the center frequency of $1/2T_f$, instead of the displacement response that

peaks at zero and vanishes at $1/T_f$. When one uses a Gaussian shaped displacement pulse (a half-width of 0.22 μs; Appendix 2, Fig. A2a), its FFT gradually vanishes without multiple zero points as can be seen in Fig. A2b. Note the half-width is 2 MHz, equaling the inverse of the base width of ~0.5 μs in Fig. A2a. The derivative of the Gaussian pulse is known as a Gaussian mono-pulse and is shown in Fig. A2c. The FFT pairs of Gaussian mono-pulses of 0.2 to 2 MHz are shown in Fig. A3. It is evident that these pulses are broad and one can hardly use the spectra for source discrimination. Even recent AE modeling efforts have not taken these points raised here and reevaluation is called for.

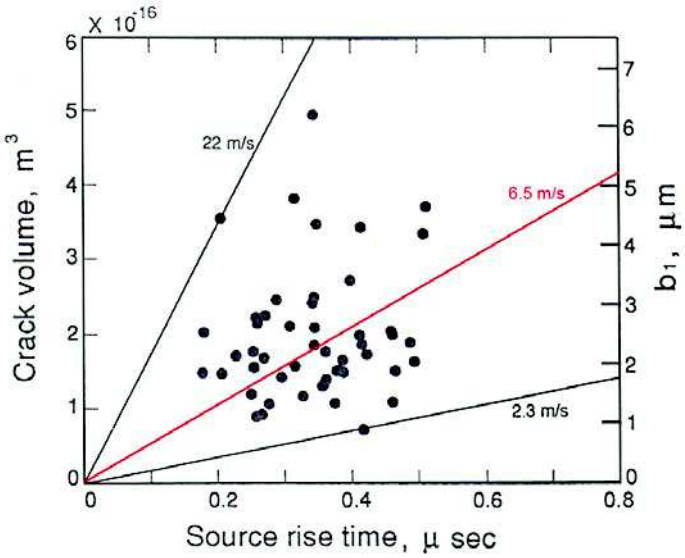

Fig. 6 Crack volume vs. source rise time. Data points are within the zone between crack velocities of 2.3 and 22 m/s. [71]

Still another issue evolves from the examination of Fig. 5. Note the three waveforms originated from fiber fracture, but with different propagation paths and distances (6.2 to 12.2 mm). These differences resulted in P, SP and S waves arriving at variable timing. Typical argument for the frequency contents relies on the P-wave arrival. However, a sensor detects all arrivals and time differences dictate the frequency spectra of the received AE signals. This aspect must be accounted for as well in discussing the frequency content of an AE signal when it consists of bulk waves.

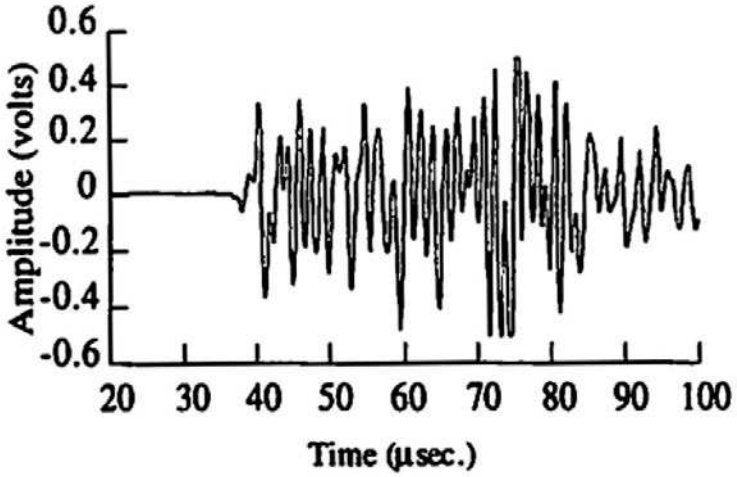

Fig. 7 Typical waveform from a transverse matrix crack in $[0/90_n/0]$ CFRP. [77a]

Matrix and interfaces

AE signals originating from the matrix and interfaces are varied and range from weak to strong, making unambiguous characterization difficult in practical composite structures. Several different mechanisms are expected to overlap as well. In model composites, however, clear distinction is possible.

Transverse matrix cracks: In 1979, as a part of an extensive investigation on composite failure mechanisms, Bailey et al. [76] first reported using AE for detecting transverse crack initiation in GFRP, while CFRP produced no AE due to pre-failure degradation. Prosser [77a] reported one-to-one correlation between observed S_o Lamb wave signals and transverse matrix cracks in cross-ply composites (Fig. 7) when 90º-ply thickness exceeds 0.4 mm (3 plies). Notice that this signal is of high-frequency type (~700 kHz) and in thick cases (>6 plies) of very high amplitude (>80 dB). Gorman and Ziola [77b] showed even stronger events in $(0/90)_s$ CFRP, ranging up to 98 dB, but with >100 μs duration. [Note this work is the first to exploit the plate wave characteristics of AE signals in typically thin composite samples.] Some of these signals with short duration are hard to differentiate from fiber-break signals. When transverse matrix cracks occur, three possible micro-mechanisms exist; i) matrix (resin) cracking, ii) debonding of fiber-resin boundaries and iii) fracture of bridging fibers. Matrix is low strength and slower fracture produces only low energy (amplitude) AE. See [39] for epoxy cracks having ~55 dB AE even for large area cracks. Matrix cracks are present in notched woven-roving fracture surfaces in [36, 37] as resin-rich areas of the size of roving diameter exist throughout the composite. In laminates made from UD prepregs, only the interlaminar layers have contiguous resin constituent and the contribution of mechanism (i) is limited. Debonding is expected to be the main mechanism for the transverse matrix cracking in laminates with straight fibers and as the source of first ply failure. Mechanisms i) and ii) typically coexist in woven composites [36, 37]. Woo and Choi [78] characterized debonding AE to have low amplitude (under 70 dB) and low frequency (lower frequency peaks than the sensor resonance of 265 kHz for PAC μ30) using *in situ* microscopical observation of the notch-tip zone. They showed, however, that once macro-cracking begins, higher amplitude/frequency (>70 dB, 430-450 kHz) peaks are dominant, implying bridging fiber failures contribute substantially. Fracture surface showed both of these (ii and iii) mechanisms. Elevated temperature exposure (wet or dry) affects the matrix-bonding behavior, which was detected with AE. Schoßig et al. [79] used environmental SEM to assess damage mechanisms of short-fiber GFRP and identified 14 different mechanisms and recorded AE simultaneously. However, too many processes occur together. No clear correlation to AE signal characteristics is established so far. Bussiba et al. [80] exposed CFRP (0/10 layup) to 100ºC for 2 weeks and saw accelerated debonding with the knee strain down from 1.5% to 0.6%. Wet exposure of GFRP was reported in [61c, see also 81].

Godin et al. [82-85] made a series of well-designed studies using UD, angle-ply and cross-ply composites with advanced pattern recognition analysis. Using Kohonen map and k-means methods, they identified four distinct signal types and attributed them to matrix cracking, interfacial debonding, fiber fracture and delamination. Waveforms of the 2nd and 3rd types are visually indistinguishable, however. The use of Kohonen maps appears effective in identifying clusters of AE signals and will be examined in a later section. In de Oliveira's thesis [40], he summarized nearly 20 other AE works on transverse matrix cracking and also reported own cross-ply GFRP testing [see also 60]. He developed artificial neural networks based on self-organizing maps with waveform and wavelet-transform data as input. Among six clusters identified, transverse matrix cracking produced two types of AE signals having characteristic S_o waves centering at 350-400 kHz lasting 30~60 μs. The low frequency part arrived first as expected for S_o waves. Shorter

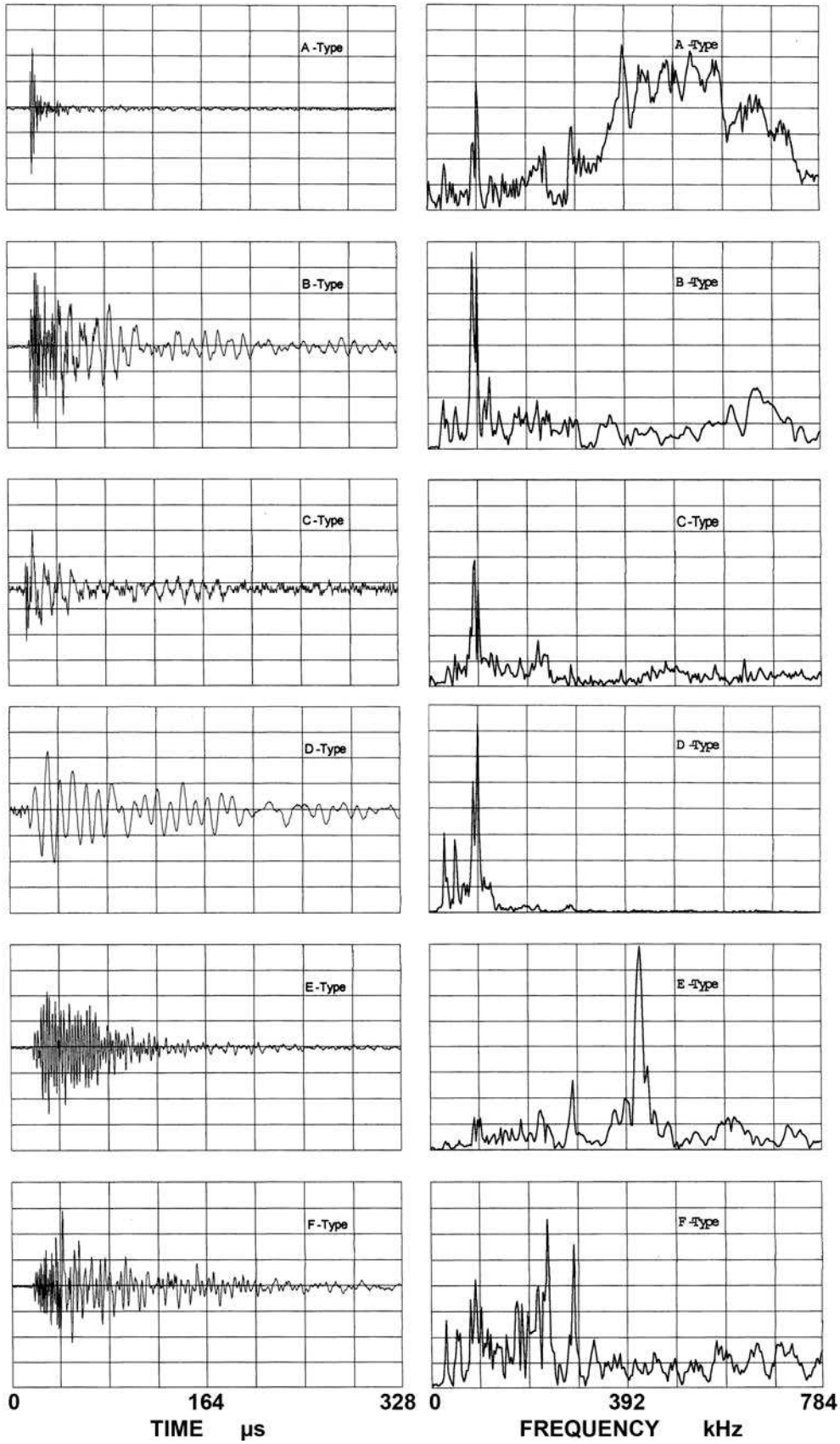

Fig. 8 Waveforms and frequency spectra of 6 different types, classified by pattern recognition analysis of AE signals from QI CFRP laminate. Time scale: 41.0 µs/div, Frequency: 97.7 kHz/div, Amplitude scale varies. WD sensor at the sample center. Huang [61b]

duration signals (type II) are attributed to the initiation, while longer ones (type I) to the propagation of transverse matrix cracks [60].

Delamination-Shear: Ono [48] reported AE from the delamination of UD CFRP with pre-cut plies with several different shearing zones. Shear strength level was 5 – 24 MPa. Overlap length ranged from 25 to 75 mm (13 mm width). Tensile loading produced initially medium amplitude signals (50 - 70 dB) with an average event duration of ~120 μs from the initiation of Mode II delamination. At higher loads, high amplitude events (70-130 dB) of long (> 200 μs) event duration were found. These are caused by rapid advances of delamination under mainly Mode II loading with out-of-plane stress near cut edges. Lagunegrand et al. [86] examined free-edge delamination on ±30º angle ply CFRP and identified 90-100 dB signals as Mode-III delamination induced AE. This delamination occurred between +30º and –30º plies in shear, while mixed mode shear was reported in $[15_n/90_m/\text{-}15_n]_s$ laminates. Scholey [87] examined delamination in large-sized QI CFRP samples with cut plies, getting 10-50 pm A_o-wave amplitude as the area of delamination reaches ~30 x 50 mm after loading. Surprisingly, duration is only ~100 μs, implying delamination expands in small steps. Huang [61b,c] examined waveforms of various AE origins of CFRP tensile samples (UD, cross-ply, quasi-isotropic) in conjunction with pattern recognition analysis. One of six types identified is due to delamination, which becomes active just prior to sample failures. As shown in Fig. 8, type-D delamination signal has the lowest frequency content (~100 kHz) and long duration, while fiber-break AE (types A and B, latter with larger matrix debonding) has highest frequency content and short duration. (Type C is from transverse matrix crack with ~100 kHz peak, type E from splitting with ~400 kHz peak and type F from shear crack in ±45˚ plies at medium frequency.) Corresponding power spectra show features originating from WD sensor resonances (esp. at ~100, ~230, ~300 and ~400 kHz) as the sensor primarily detected signals under its face in the middle of a narrow sheet sample. Effects of Lamb wave types may be present for types A and D, in particular.

De Olveira [40, 42] identified two types (IV and V) of delamination-induced AE signals in cross-ply GFRP tests. Both are A_o-mode waves with low frequency contents under 400 kHz (down to 20 kHz in type V) and strongest contents at 150-230 kHz. Type IV was observed at lower loads, attributed to matrix-fiber decohesion as well as delamination. Type V appeared near final fracture when delamination activity was high.

Delamination-Opening: Bohse and coworkers [88, 89] studied Mode I (crack-opening type) delamination using DCB specimens and correlated AE energy with strain energy release rate (G_{Ic}), supporting the concept of damage zone concept ahead of the crack tip. They consider the presence of matrix cracking and matrix-fiber interfacial debonding, the latter in stronger interface condition. Some bridging fiber fracture is possible as well as in [78]. This also has more high frequency component, allowing the discrimination of the two mechanisms. In both, however, the main frequency feature is the dominant low frequency components below 200 kHz. Amplitude of these AE is mostly (~90%) in 60-80 dB range. Another CFRP DCB tests [64] reported essentially same results with a comparable low frequency peak (120 kHz with minor one ~300 kHz, both characteristic of WD sensor). This low frequency peak was also seen in epoxy resin crack and in lap-shear AE.

Recently, Sause et al. [53] published a comprehensive study of DCB tests with AE analysis examining interlaminar crack propagation in GFRP and CFRP. They conducted pattern recognition analysis to identify three clusters, corresponding to matrix cracking, interfacial failure and fiber breakage, using mostly frequency-based features, such as average, centroid, initiation, peak,

weighted peak frequency, six partial powers, etc. Cross plot of partial power at 450-600 kHz vs. weighted peak frequency easily separated the 3 clusters. Figure 4 in [53] compares observed and FEM-simulated signals and wavelet spectrograms, showing good agreement. Interfacial failure dominates cumulative signal amplitude, followed by matrix cracks. Fiber breaks contribution is low as this comes from bridging failure. This theory-test-model hybrid approach holds great promise in assessing complex structural composite design under various loading conditions, integrating AE as a part of health-monitoring scheme.

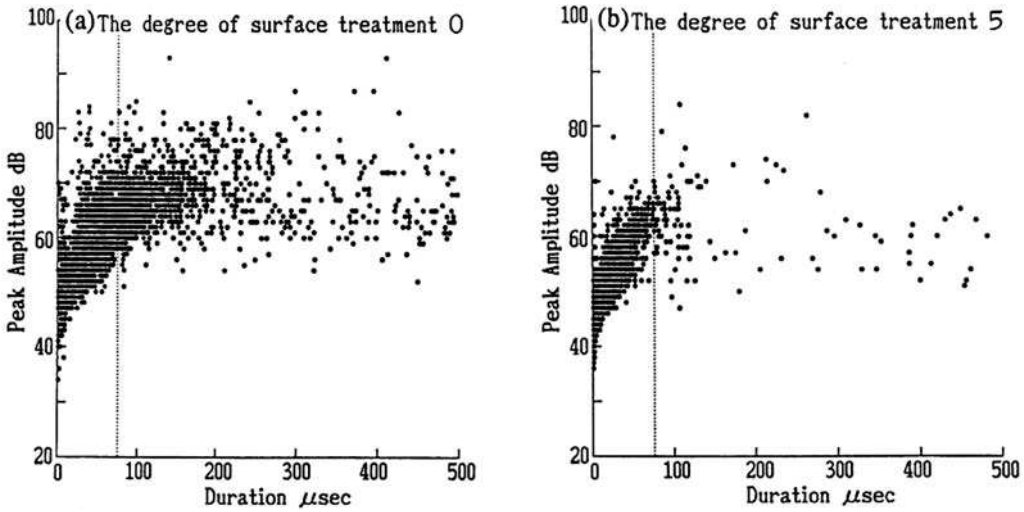

Fig. 9 Amplitude vs. duration of tow-composite samples with (a) no and (b) maximum surface treatment. [44]

Fiber-pullout: In tow composite tests, Nanjyo [44] used 4 different levels of (pitch-)CF surface treatment. Without treatment (level 0), many fiber pull-outs of up to 100 μm were observed after failure. With maximum treatment (level 5), fiber-matrix bonding improved and few fiber pull-outs were found producing flat fracture surface. Comparison of these two conditions on amplitude-duration plots indicates events with 60-80 dB amplitude, longer than 80 μs duration increased more than ten-folds in the level-0 sample. These long duration signals are due to fiber pull-outs. This means pull-out AE amplitude is 9 dB higher to fiber fracture (Fig. 9) on average. However, differentiation must rely on duration. Single glass-fiber pull-out experiment by Mielke [90] produced similar results regarding amplitude, though fiber diameters of 20-25 μm were used and fiber-break amplitude was ~10 dB higher than pull-out signals while another study examined pull-out of SiC fiber from glass matrix [91]. A more recent work used AE in single Kevlar-fiber pull-out tests, and showed energetic signals of 50-90 dB (Pico sensor). However, AE part is difficult to evaluate lacking key details [92].

Mixed mode cases: Mizutani et al. [93] examined fracture of cross-ply CFRP under central point loading and observed four separate types of AE signals. Signal simulation using laser sources allowed him to establish source mechanisms of fiber fracture, transverse crack, delamination (shear) and matrix crack, designated as type-A, -B, -C and -D. These 4 signal types are shown in Fig. 10 together with wavelet spectrograms. Two sensors placed at 90º angle from the loading point (along 0º and 90º relative to the surface fiber axis) showed vastly different waveforms, helping the identification process. Of 327 total, initial 70 events showed the following: Mode-I type fiber fracture in the front layer (the first event + 3), followed by transverse matrix cracks in the mid-lamina (27), from the middle part on, delamination (15) and splitting-type matrix cracks (11), (13 unidentified). They also studied the same experiment, but under dynamic loading

condition. Details can be seen in JAE [94]. Four types of cross-ply CFRP plates were impacted. Lamb-wave AE signals were detected by small AE sensors on both surfaces to separate S_o and A_o modes. Only Impact-AE is obtained when the impact energy is below a fracture threshold. When internal fracture occurs, both Impact-AE and fracture-induced AE (or Fracture-AE) were detected. Most of strong AE signals were correlated with splitting matrix fracture source (type D in Fig. 10).

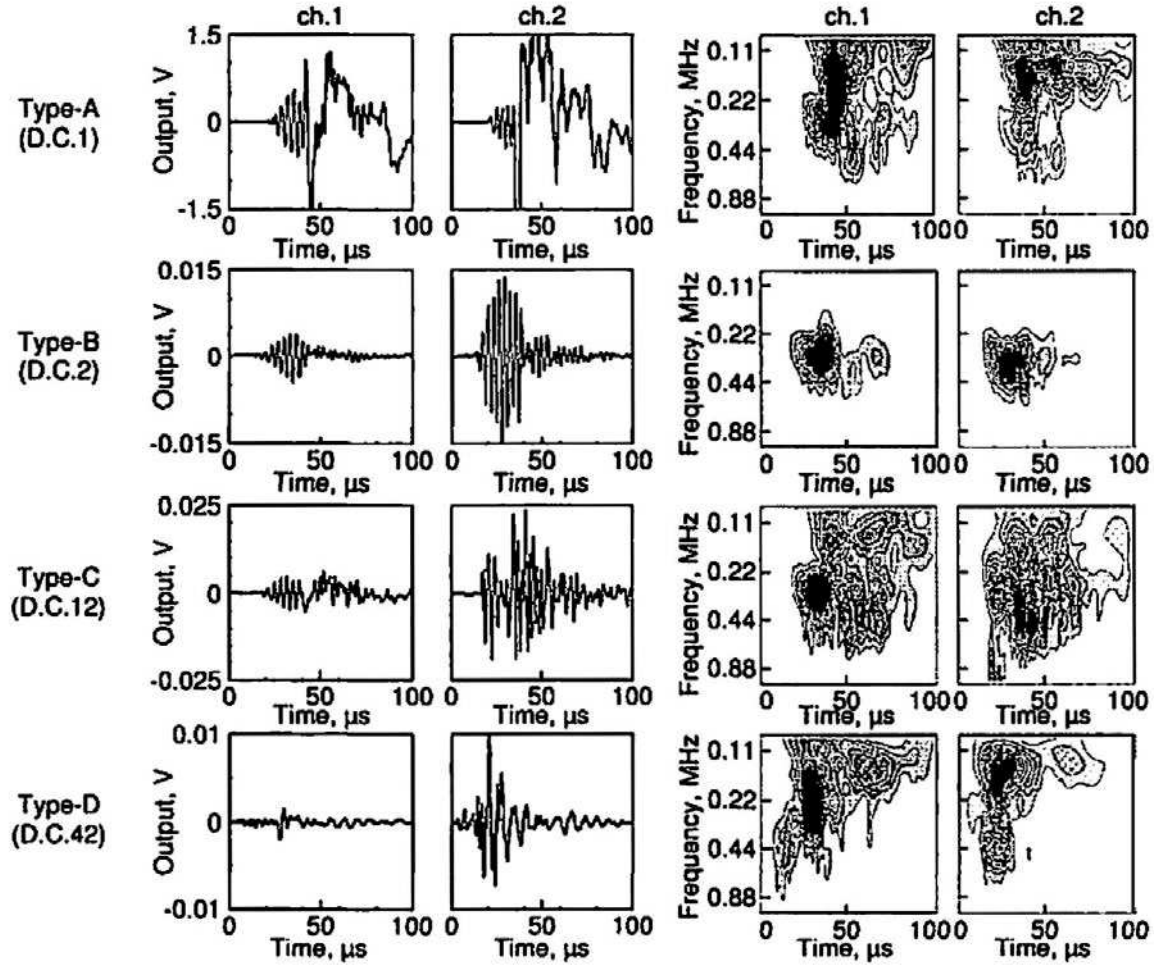

Figure 10 Waveforms and wavelet spectrograms of 4 types of signals from point-loaded cross-ply CFRP. [87]

There are other types of matrix fracture. For example, matrix fracture similar to the transverse matrix crack, but fibers oriented along the loading direction, also occurs. This is usually called splitting and corresponding waveform is that of type E in Fig. 8 [61b,c] (also type III in [40, 42]). Another type of matrix fracture occurs under shear stress along the fiber-matrix interfaces in angle plies, such as those ±45º plies in quasi-isotropic laminates. This has a characteristic waveform of type F in Fig. 8. Both E and F types have slowly rise time, reflecting slower growth of such cracking (WD sensor was on top of these sources 0.5 mm away, so no propagation induced slow rise time). The characterization of signal types relied on the laminate types and when these signal types were emitted during loading. (Note these features are dependent of test conditions: these tests used thin (~1 mm thick), narrow (13 mm wide) CFRP samples with WD sensor attached at mid-section. See also [95].)

Felicity effects

When damage accumulates in materials, Kaiser effect breaks down. This is usually characterized by Felicity ratio; the stress of AE restart/prior maximum stress. Felicity ratio has been linked to the residual strength of composites, and has been studied over many years: see Hamstad's thorough discussion in 1986 [96]. Changes in Felicity ratio on laminates are shown in Fig. 11a and b. In Fig. 11a, Hamstad [96] shows a schematic plot of GFRP data by Fowler and Gray [10], where it drops with applied load. Awerbuch's data on a multi-ply CFRP decreased with increasing prior stress above 1/3 of the tensile strength of 272 MPa [97]. Felicity ratio was down to 0.7 with prior stress of 220 MPa or 80% of the maximum. These are data from tensile coupons. On bend testing, GFRP also exhibited Felicity effect, but stress level at the start of decreasing Felicity ratio is higher (75-80%) instead of 45-60% in Fig. 11a, as shown in Fig. 12 [98]. Obviously, the difference arises from different failure mechanisms between tension and bend tests, but exact cause is unknown. AE monitoring in compression-after-impact or bending tests with damages showed the reduction of FR values [e.g., 99, 100]. Various AE parameters including FR were combined with neural networks for burst pressure prediction [e.g., Hill, [23], pp. 382-387].

The origins of Felicity effects need to be explored further as we find few articles beyond Hamstad [96]. It is obvious that the stiffness of fiber-damaged zone is reduced and stress/strain differentials develop against the surrounding sound zones upon reloading. This is realized during any unload-reload step [cf. 41], since the stiffness is proportional to the fraction of intact fibers. A damaged zone has a lower stiffness and deforms more. The stress/strain differentials, in turn, produce additional interlaminar stresses, leading to premature delamination. This can be the source of Felicity effect in impact-damaged vessels. In the absence of fiber damage, delamination itself should give rise to frictional AE during an unload-reload step. At any interlaminar, resin-rich layer between plies of different fiber orientations, interlaminar shear stresses are always present. While the shear fracture strain is of the order of 1% in most resins used today, it is common to use longitudinal-hoop fiber angles of 60-70º and substantial interlaminar shear stresses result upon loading. With our current AE methods, separating delamination and frictional AE signals is feasible. With the above scenarios for Felicity effect, we should expect strong FR dependence on lay-up sequence.

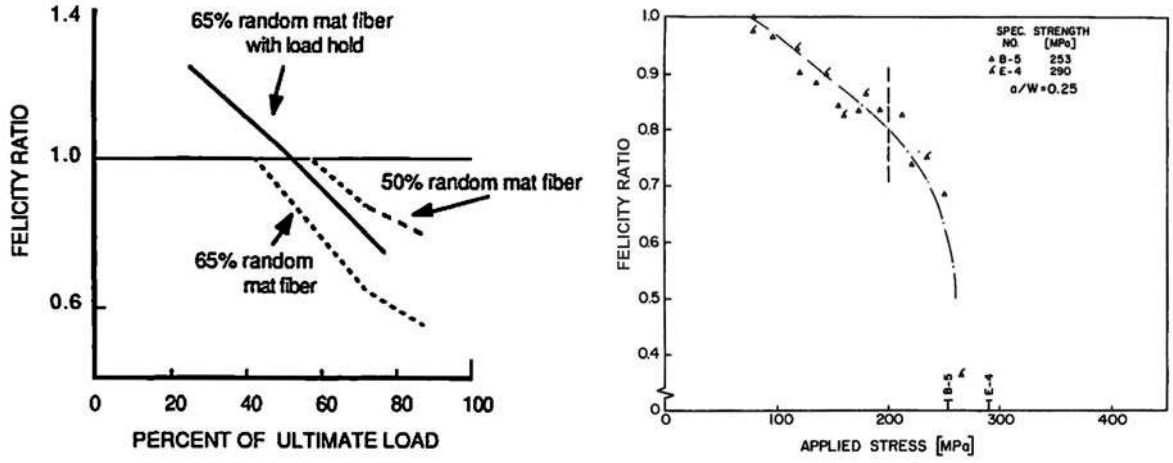

Fig. 11 a) FR vs. applied load of GFRP [96]. b) FR vs. applied stress of multiply CFRP [97].

Felicity ratio (FR) provided sensitive measure of developing damage under compressive tests [101]. CFRP laminates with 914 or PEEK resin matrix having a seeded defect were cyclically loaded and f = 1 – FR was used as damage indicator (of internal delamination). Applied load P

and f are related with laminate specific manner with high R^2-values >0.98. See Fig. 13. As the marks for visible crack indicates, f-value gives the warning of internal damage.

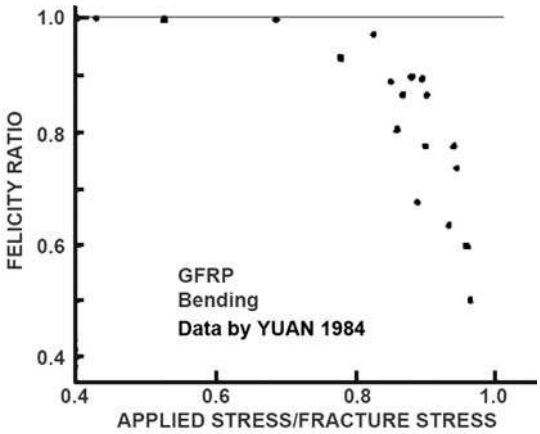

Fig. 12 FR vs. stress ratio of a GFRP under bending load [98].

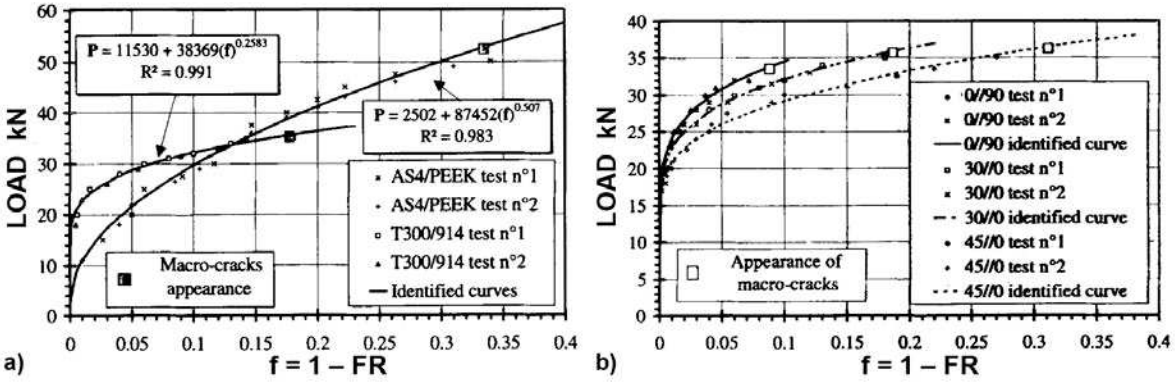

Fig. 13 Cyclically applied peak load vs. f = 1–FR for CFRP. a) with different resin, b) different orientation [101] Loading is compressive and CFRP has an internal defect to initiate delamination. Appearance of macro-cracks is marked by squares.

Several stressing sequences are used in obtaining FR. The usual one is to unload from the previous maximum as in [101], whereas incomplete unload sequences are more convenient to perform. One such example is shown in Fig. 3, called intermittent load hold (ILH), while CARP procedure calls for 10% unload with stepped loading (Fig. 4, [15]). The origin of Felicity effects is most likely from frictional (secondary) AE [97], but the link between Felicity effects and residual strength is empirical. Toward clarifying this link, NASA has embarked on extensive basic study of FR as they view this as one key element in the prediction of composite over-wrapped pressure vessel (COPV) performance. Specifically, it was found that some COPV failed in accelerated stress rupture testing; that is, COPV is pressurized and held for extended periods. They cannot afford such a failure in space [102]. Tow composite tests using Kevlar 49 and IM7 and T1000 carbon fibers were initiated with 4 sensors mounted on 250 mm long samples [55, 103-105]. AE results for a T1000 tow test was seen in Fig. 3. FR from this and similar tests showed quite different behavior compared what we have observed previously. Figure 14 shows the new findings. Data for an IM7 COPV is also included for comparison. Felicity ratios given here were determined using the first AE event for Kevlar-epoxy tow, and the mean of the first 15 events for T1000 tow, IM7 tow, and the single IM7 COPV. FR values are in all 4 cases higher than 0.9 even very close to the failure load. FR is above 1.0 up to load ratio of 0.6-0.7 for CF and 0.85 for Kevlar fiber. For COPV, FR stays above 1.05 to load ratio of 0.78. First, these finding again

imply that fibers remain intact to much higher stress levels than older CFs like G50 used in [48] (IM7 is relatively old, however) as discussed earlier in conjunction with Fig. 3. A recent study [106] of T1000 Weibull modulus indicates that m-value at lower strength range exceeds 30 (overall m = 5.9), thus virtually eliminating fiber fracture below 80% of the average strength. Second, frictional mechanisms are not as active as in old CFRP, reflective of better interfacial bonding. Interlaminar shear strength has doubled from previously common AS4/3501 (76 MPa) to newer T1000 CFRP (150 MPa). This condition is true even in COPV, in which windings of various orientations are expected to lead to interlaminar shearing and friction (it is unclear if this particular COPV was subjected to autofrettage* (*an over-pressurization step to put the metal liner in compression), which can suppress AE at lower loads.) Third, flaws like splitting or delamination are not expected in tow composites, although this is not the case for COPV. As higher FR values are linked to low damage state and higher failure strength, more extensive studies on composite Felicity effects seem to be highly advisable. These should point to improved materials and manufacturing processes. FR on pressure vessels will be discussed later.

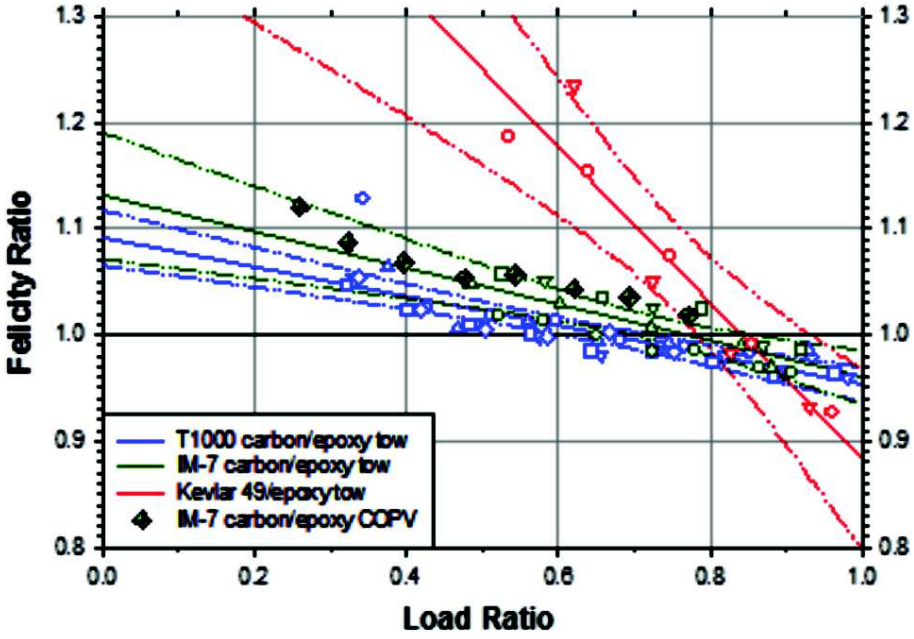

Fig. 14 FR vs. load ratio for T1000 carbon-epoxy tow (black-dotted), IM7 carbon-epoxy tow (grey-dashed), Kevlar 49 -epoxy tow (white-solid lines), and an IM7 composite overwrapped pressure vessel (large crossed hexagonal symbols). 95 % confidence intervals also shown. [105]

Wave propagation

Typical composite structures comprise thin members and AE signals are transmitted as Lamb or plate waves of extensional (or symmetric) and flexural (asymmetric) modes. Many composite members are anisotropic as well. Basic aspects on plate waves have been covered well in [12] and standard textbook [107]. In composite AE field, work by Gorman and coworkers [108-110] brought the focus on the peculiar wave propagation behavior of AE signals in thin composites, especially on the aspect of source orientation producing different wave modes. Hamstad and his NIST colleagues enhanced our understanding with extensive finite element modeling studies to shed light on the source types and resultant plate waves [111-114]. Large wave attenuation in composites has been accounted for in CARP methods [8-17, 20, 21]. Downs and Hamstad [115] showed the sharp amplitude drop (20 dB in 6 mm) due to geometrical spreading in CFRP vessels of inverse-square-root distance dependence. More recently, the anisotropic nature of composite plates has been included in analysis. Mal et al. [116] used a classical damping factor approach to

anisotropic wave analysis and found satisfactory results between theory and experiment (though this work is difficult to transfer to AE study). Sause incorporated suitable source models and wave propagation analysis on such CFRP model sheets [53, 69, 70]. Using complex elastic modulus obtained by air-ultrasonic technique [117, 118], some wave propagation analysis included attenuation factors as well [119-122]. Anisotropic velocity calculations are also reported for common CFRP layups [123-126].

Actual measurements of attenuation are limited. Suzuki [71b] measured P-wave attenuation in 60% UD-GFRP as a function of propagation direction and frequency. Along the fibers (at 0˚), attenuation was 60 dB/m for 0 – 1 MHz and 180 dB/m normal to fibers (at 90˚), 0 – 1 MHz. See Appendix 3. Suzuki also showed the relaxation function model of Weaver [73] fits the data above 1 MHz, but measured attenuation did not diminish at low frequencies contradicting model prediction. Prosser [76a] obtained apparent attenuation of S_o and A_o waves in IM7/977-2 CFRP of 1.2 and 3.7 mm thick quasi-isotropic laminates. For S_o mode in the thinner plate, attenuation was 42 dB/m (410 kHz) and for A_o mode it was 83 dB/m (85 kHz). For the thick plate, corresponding values were 35 dB/m (230 kHz) and 51 dB/m (90 kHz), indicating the effect of thickness and frequency. Attenuation observed on a CFRP pressure vessel [115] was higher. These values change when geometrical spread of inverse-square-root (Lamb waves) is accounted for. Gallego and Ono [127] reported attenuation measurements on CFRP plates of three types of layups (UD, XP, QI). S_o and A_o wave modes are separately evaluated and frequency effects are examined. Attenuation is also high. It is evident that any AE analysis must consider frequency-dependent signal loss through the transmission. It must be pointed out that some of theoretical papers on Lamb wave attenuation [117-126] state that guided waves propagate long distances. This is contrary to their results, many showing 100+ dB/m, and without experimental support.

Applications

Pressure vessels and tanks - 1

When AE applications mature, we find few reports in publications especially after these are compiled in reference books, like NDT Handbook [23] and codes and standards established. Applications to chemical tanks and vessels fall into this category after the first three AERC/AECM conferences [24a-c]. Rocket motor case applications are at a similar state [see [23], pp. 377-381]; actually, few reports had appeared from the beginning due to their sensitive nature. In this connection, it is interesting to find a review on the burst pressure prediction; Joselin [128] covers the subject quite comprehensively, introducing each paper adequately without inserting own interpretation. Thus, a reader must judge which approach is successful/unsuccessful on his/her own. Also many papers from AECM series conference proceedings are missing, as access to them may be difficult outside the US. Still this review is a recommended reading on this topic.

There are two important issues at this time. One is the evaluation of impact damage and the other is estimating the residual life of COPV. The first topic is not limited to pressure vessels, but it is one of the critical problems in aerospace circle. This has been studied with AE for more than 20 years [e.g., 129-135]. It is known that impact energy links to the burst pressure. Many AE parameters have been "successful" in predicting the burst pressure [23, 128]. An example of burst pressure-Felicity ratio correlation is shown in Fig. 15 [130]. While the sample size of this study is small, it is believed a larger database has been prepared to show the same trend within the aerospace circle. Yet industrial practice still uses AE as a supplementary method. As a tool for space COPV inspection, Chang [136] in 2003 assessed AE to be *better* on "inspection time" and "field use", as *average* on "flaw characterization", "simplicity" and "COPV preparation" and

as *weak* on "whole field", "data evaluation" and "sensitivity". In the AE field, we think "whole field", and "sensitivity" as AE's major strong points, but actual judgment by the practicing engineers is much more critical.

As mentioned in *Felicity effect* section, NASA is attempting to use AE for COPV burst pressure prediction [102-105]. This is now based on the higher levels of newly measured FR values of near unity. Figure 16 shows Felicity ratio with increasing previous highest pressure for an IM7 COPV during two separate pressurizations to 6800 psi (circles) and to burst (crosses). A linear fit is made to both pressurization data. Once the FR value at burst is established with confidence, this will allow burst pressure prediction from lower pressure ILH loading schedule. As noted before, this FR-pressure relation is comparable to tow composite behavior. This surprising similarity is promising in a sense that newer COPV manufacturing is eliminating many sources of flaws that previously decreased FR values, and also reduced COPV strength. It is hoped to see even better correlation develops in the case of newer T1000 fibers.

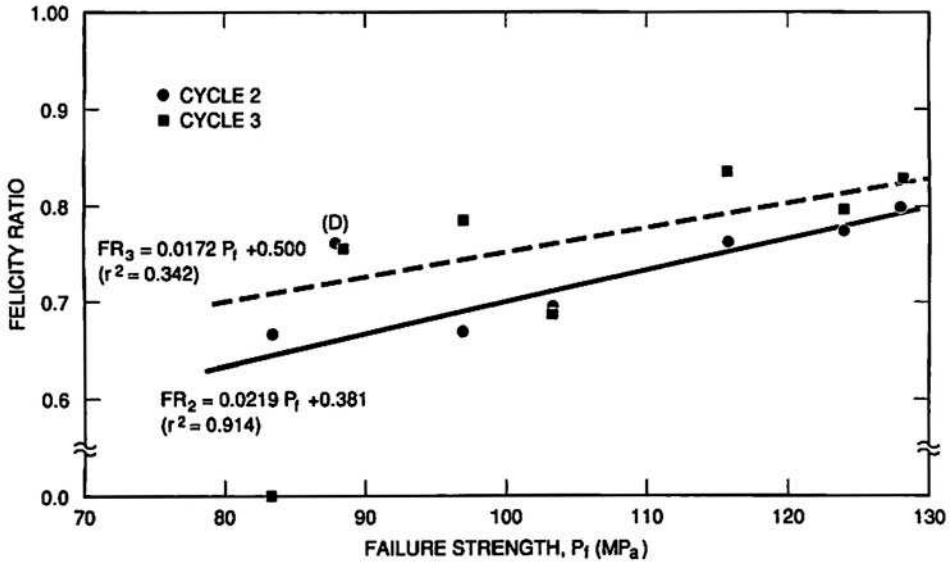

Fig. 15 FR values are almost linearly related to failure strength of spherical Kevlar COPV [130].

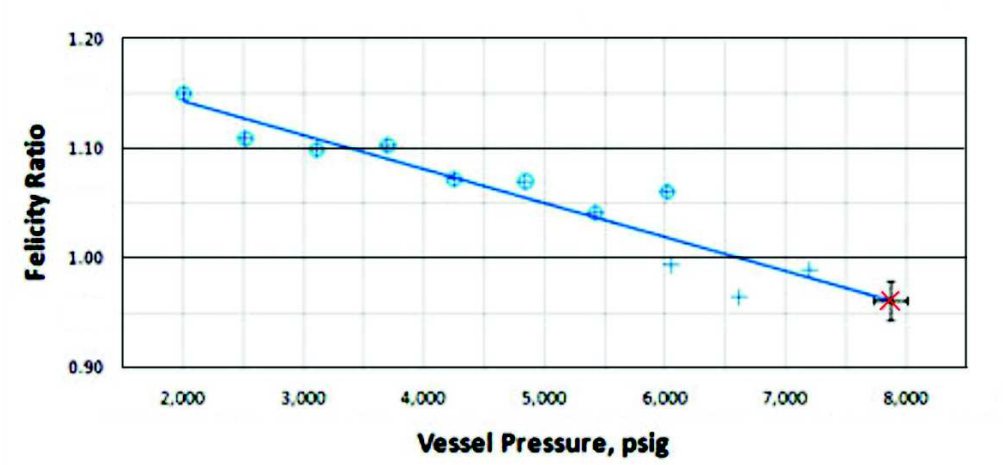

Fig. 16 Felicity ratio vs. increasing previous highest pressure for an IM7 COPV. Data from [105].

In connection to the use of FR values, it should be noted that another parameter is useful in some cases. Downs and Hamstad [133] defined Shelby (countdown) ratio, which is (the load

during unload when a predefined AE activity level is reached) divided by (the previous maximum load). This ratio was used much like FR values in correlating to the burst strength of CFRP pressure vessels. This ratio is being used in the NASA study discussed above [102-105].

The second problem of estimating the residual life of COPV comes from stress rupture behavior of high strength fibers. It is well known that silicate glass suffers from static fatigue, i.e., time dependent fracture due to the presence of moisture, aka. stress corrosion cracking. Similar effects exist in COPV made with Kevlar and carbon fibers. Figure 17 shows sustained load design curves for three types of COPV. These are used for determining the allowable sustained-load operating stress for a specified time at load using a probability of survival of 0.999. The time at pressure represents the sum of the time that the COPV is pressurized at or above 60% of mean expected operating pressure [136]. Over a long period of service, allowable applied stresses are quite low relative to the static strength. Of the three fibers, carbon fibers give the best performance at longer times (>100 hrs).

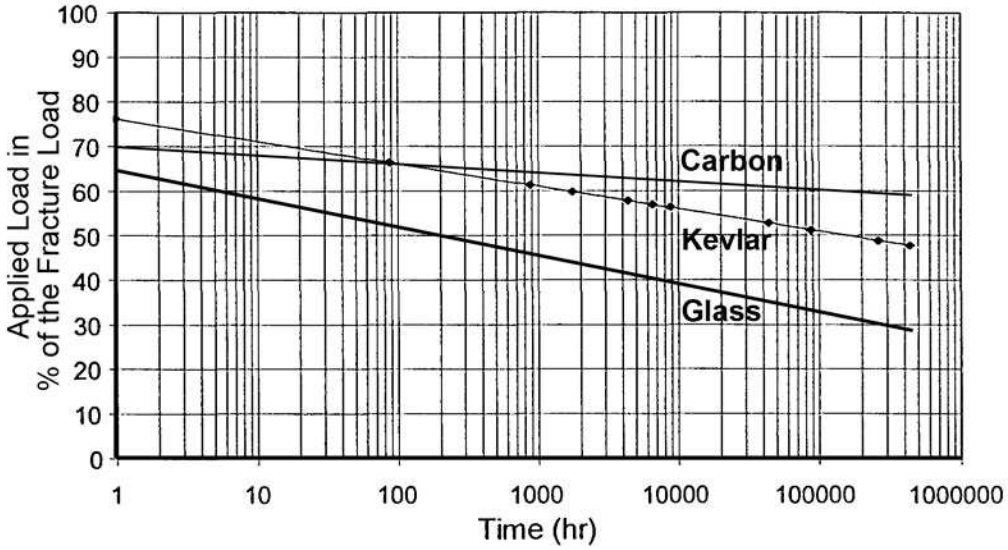

Fig. 17 Sustained load design curves for three types of COPV. Data from [136].

Since fiber fracture is the root cause, AE can play a significant role in resolving this problem of estimating the residual life. From the earliest days of AE, the stress rupture issue was recognized and Liptai [5] reported the process of stress rupture of a GFRP NOL ring. See Fig. 18a, which follows two hrs of loading before fracture with rising AE counts. This sample was loaded to 80% of the expected fracture load. Another NOL ring was loaded in fatigue at 50% of the ultimate load. At each 2000 cycles, it was loaded to 75% with AE monitoring, shown in Fig. 18b. As listed in the figure, estimated FR values decreased with loading cycles, quickly dropping to ~0.5 (as noted earlier in Introduction). Since then, however, only a few reports of AE monitoring of stress rupture of FRP appeared in the last 40 years [136-140]. There are reports of FRP stress rupture studies [e.g., 141-143]. NASA conducted wide-ranging study of Kevlar COPV used in Space Shuttles (24 used in each orbiter vehicle) after the Columbia accident and reestablished the reliability to be 0.998 relying mainly on accelerated pressurization testing. Raman spectroscopy was used to evaluate the residual stress state of Kevlar [144]. No mention of AE appeared in the report. However, another program is in progress [55,102-105,140] at NASA. On stress rupture tests, only a glimpse of data can be viewed so far [145], showing the usual increase in AE just prior to failure. In some cases, other data appear inconsistent [140] and we need to wait for the completion of the program. Still the location data on a successful test of a COPV shows several

concentrations of energetic AE events within 24 hrs of final failure (slide 19, [145]). Two views are given in Fig. 19. Such data point to the availability of information that warns incipient failure if continuous AE monitoring is used. Without monitoring, projecting 0.999-level reliability will probably require a new strategy yet to be formulated.

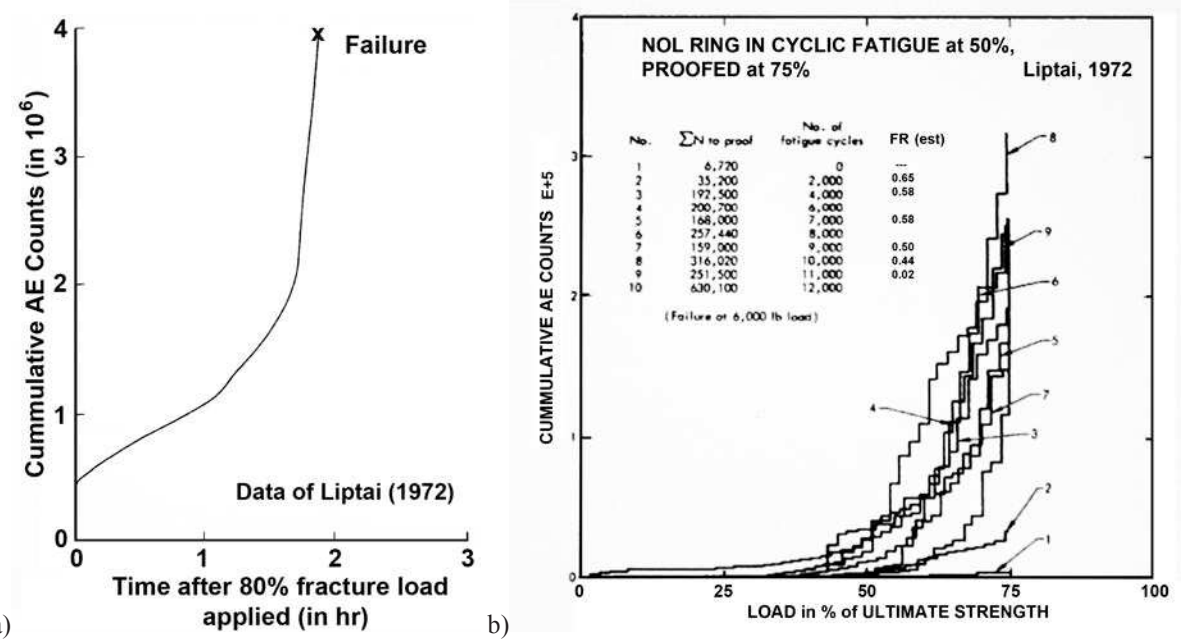

a) b)

Fig. 18 a) Cummulative AE counts vs. time at 80% of fracture load applied. b) AE counts vs. load under fatigue load with intermittent proofing. Data from [5].

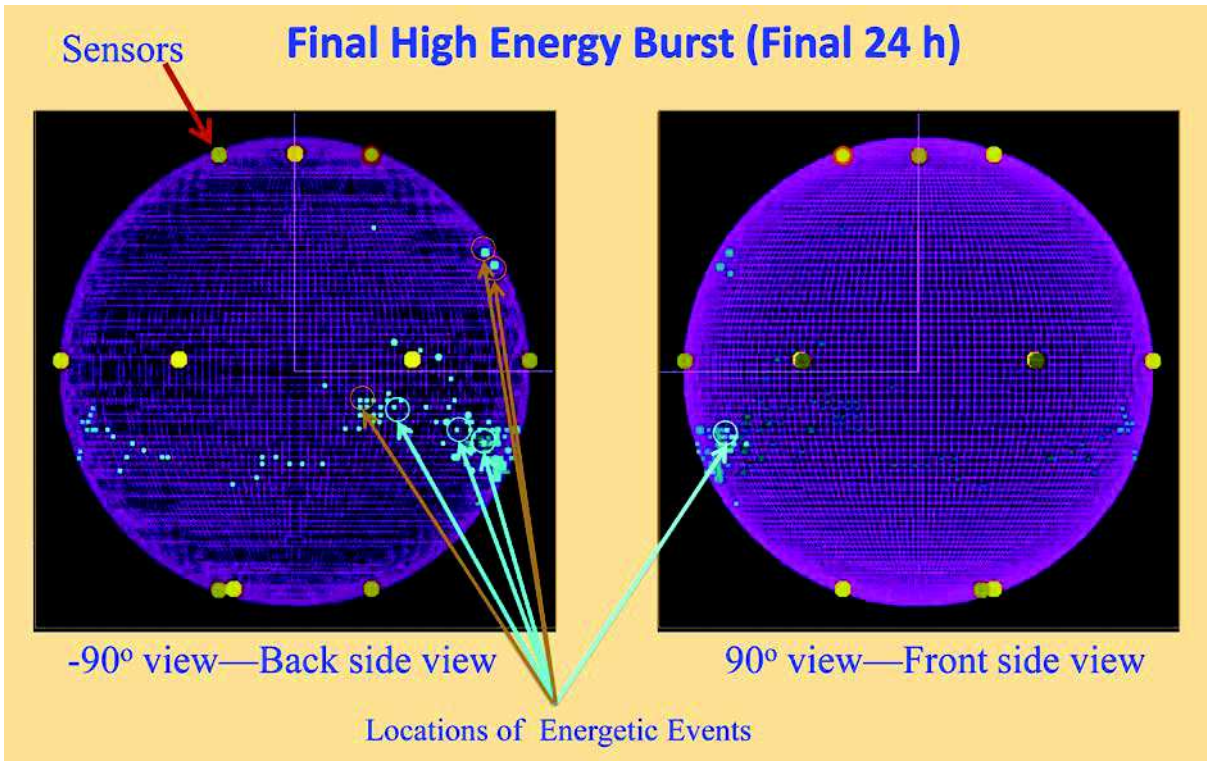

Fig. 19 Distribution of energetic AE events in 24-hrs period before the final fracture. Kevlar COPV. Data from [145] with color inverted for easier viewing.

Pressure vessels and tanks – 2

AE tests of smaller tanks have occupied some European AE groups of late. These have to be

done at low cost and rapidly. See [146-148]. A similar effort was undertaken by Propane Education & Research Council in the US, using ISO11119-3 as the basis. They chose to use only visual inspection, relying instead on the safety factor [149]. They stated in their Exemption request to the US Dept. of Transportation (prepared by Battelle) that "Electronic methods which have been examined to some level of detail in the laboratory include acoustic emission and acousto-ultrasonics (sic). Other potential inspection methods include holography, shearography, and thermography. These methods are used by highly trained staff in controlled laboratory and manufacturing plant conditions for quality control and special purpose applications. However, available data indicate the quality of damage detection in composite cylinders by these methods is inconsistent and varies significantly with the material selection, design, and manufacturing techniques. Consequently, unique NDI test criteria will be necessary for each different cylinder design, even though they may be from the same manufacturer. Practical application of these methods will be erratic and inconsistent for operations which inspect more than one cylinder type at one time, as is typically done in cylinder and propane industries." Their products, LPG/CNG cylinders, are inexpensive, requiring the lowest cost inspection method. Yet, this seems to be the state of general NDT community that is so ignorant of the state-of-the-art in AE technology. The safety factors they incorporated are still of interest; This value, minimum stress ratio, is defined as the ratio of the fiber stress at calculated design minimum burst pressure divided by the fiber stress at 2/3 times test pressure (i.e. working pressure). For cylinders without liners or with non-load-sharing liners, the stress ratios are:

- Glass fibers – 3.4
- Aramid fibers – 3.1
- Carbon fibers – 2.4

These cylinders are designed to last 15 to 50 years and the minimum stress ratio is to assure against failure due to stress rupture. Note CF can be stressed the highest. It is not known if this has received DOT approval.

On the side of chemical vessels, AE is well accepted thanks to the efforts of Dr. Fowler and the CARP, as mentioned in the Introduction. A manufacturer of FRP vessels [150] recommends AE testing of their product as follow: "Acoustic emission tests on used equipment are most effective when there is baseline information available. It is therefore recommended that all critical FRP equipment be baseline AE tested soon after start-up. Once in service, the amount of AE testing that is done is the owner's prerogative. Often, equipment is tested at a point in time approximately halfway through the estimated life span of the equipment. Ongoing testing will depend on the results of this test. When critical equipment is nearing the end of its service life, regular AE testing can provide a meaningful structural evaluation that may prolong equipment use and prevent unexpected failure. Acoustic emission testing identifies and locates active defects in laminates by detecting minute acoustic impulses that are generated as a defect propagates under load. A major advantage of this procedure is its ability to monitor an entire piece of equipment quickly." This is a welcome testimony for the validity of AE testing.

Small, but extremely high-pressure cylinders also present technical challenge, as in the case of 100-MPa hydrogen cylinders [151]. Also see Gorman [152] for AE specific discussion. A new ASME Code case was developed based on AE to provide the accept-or-reject criteria. These are based on the curvatures of cumulative events and energy curves that quantitatively measure pressure vessel stability. These are COPV, but the liners do not carry load, unlike the space counterpart discussed in the previous section (these carry 20-30% load [144]). An example of AE cumulative event (ΣAE during load hold) analysis is shown in Fig. 20. Left curves are AE events curves for 4 channels. At 320-570 s, load is held and event rates started to decline, which are fitted with exponential functions of the form

$$\Sigma AE = A \exp (B\, t) + C, \qquad (2)$$

t = time and A, B, C constants. For the curve on the right, shape factor B is –0.0183 and goodness of fit is $R^2 = 0.91$. When B is negative, AE event rates decay and the vessel is accepted as stable. Other factors used include the number of fiber breaks, fiber break energy, background

energy oscillation effect (which begins at 60-75% of burst pressure) and frictional AE. This Code is now published from ASME (Section X, Appendix 8, 2010) [151b] and being applied in the field. This Code requires for vessel acceptance that the value of B falls between –0.1 and –0.001 and $R^2 \geq 0.80$. Alternately, it is possible to use time required for the structure to emit 99% of AE events on a dwell, namely, $t_{99\%}$. Here, $t_{99\%} = \ln(0.01)/B$ and takes values between 25 and 40 min. For various non-AE requirements, see [151a and b].

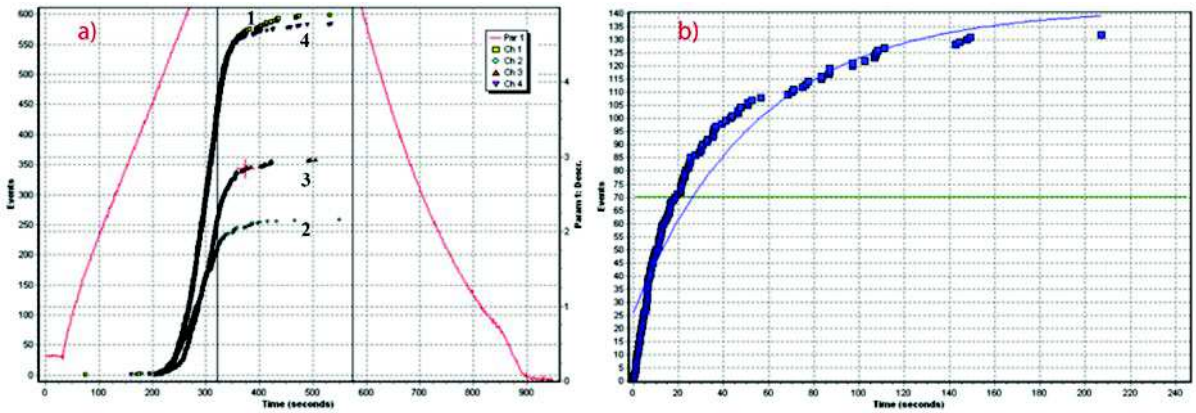

Fig. 20 a) Cumulative events and pressure vs. time. Load is held between two vertical lines. b) Exponential fitting of the cumulative events vs. time for channel 1 during pressure hold period. [152]

Wind turbines

Increasing size of wind turbine power generators demands constant monitoring and maintenance. Articles of applicable NDT methods and of AE methods have appeared [153-157]. Ciang et al. [153] reviewed various SHM methods, with a broad discussion on AE with a dozen references. Some new approaches are suggested. Reference [154] suggests somewhat limitedly "AE is considered more robust for low-speed operation of wind turbine compared to the classic vibration based methods. This approach is also more ideal for identifying early faults in gearbox bearings." Reference [155] is a brief summary, while [156] reported on an AE test of 25-m long blade with a static step loading schedule and noted locations of AE events at 77% of the fracture load. Sensor placements tightly (20-50 cm spacing) surrounded the eventual failure site.

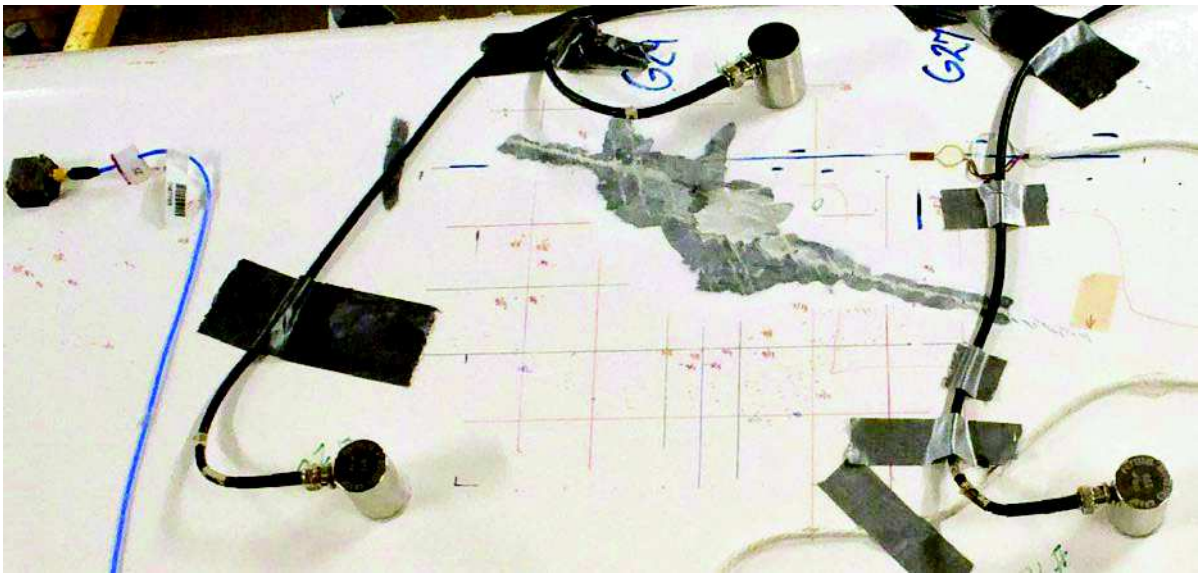

Fig. 21 Surface damage above the spar-cap skin interface with 3 R6I AE sensors (#18-20). [100]

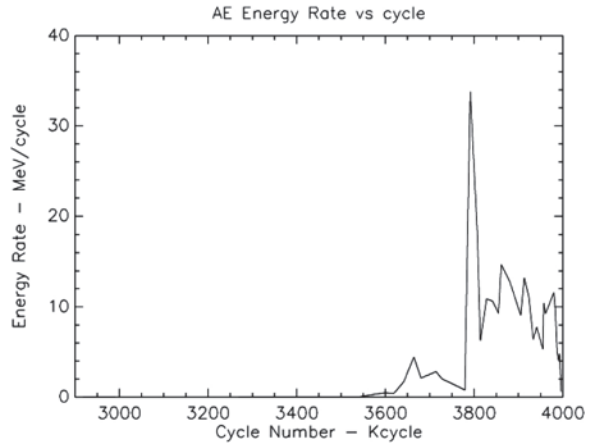

Fig. 22 AE energy rate vs. fatigue cycles. [157]

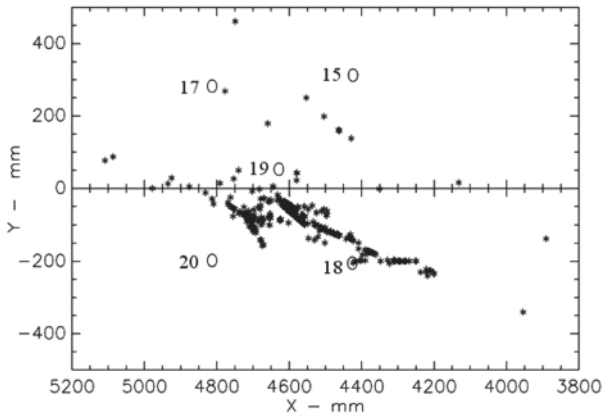

Fig. 23 AE event locations near the spar cap end. [157]

Rumsey et al. [157] conducted high-cycle fatigue loading of TX-100 blade of 9-m length to over 4 million cycles. Dr. Beattie performed AE testing portion. This blade has 6-mm balsa wood at center, a glass cloth supporting a single ply of UD carbon fibers at 20º, then the top mat layer on both sides. At mid-length, spar cap is joined to the base side, where eventual failure was predicted and AE monitored. At ~2.5 million fatigue cycles, a large visible crack developed parallel to the chord axis on the high-pressure side at ~4.5 m. The crack then grew along the 20º off-pitch-axis carbon fiber direction until the test was stopped at 4 million cycles. Figure 21 shows the surface damage above the spar cap skin interface with 3 AE sensors (PAC R6I) nearby. Almost immediately with test start, AE detected AE events and followed the evolution of blade failure around the end of the spar cap at 4.5 m, but no significant damage in any other monitored areas (24-channel system used). Significant AE appeared at 3.55 million cycles and extreme damage indications started at 3.78 million cycles (see AE energy rate in Fig. 22). The locations of the AE events (Fig. 23) matched the visual damage shown in Fig. 21. The most significant result of this test was that only AE was able to predict and identify the damage location and severity while a few other SHM sensors failed to see the damage.

Another approach for AE characterization, i.e., pattern recognition/neural network, has been used for AE signals from turbine blade tests. [158-160] This approach provided damage grade assessment, relatable to the state of cracks and other flaws developed in fatigue loadings [158]. Load-hold emissions were useful in setting up the classifiers. Other methods evaluated different aspects of blade state assessment [159, 160]. This application is still developing and new methods are expected in this Conference.

Space Shuttle

NASA tried to develop and implement on-board impact detection technologies after the loss of the Space Shuttle Columbia. Prosser [161, 162] described a system called Shuttle Wing Leading Edge Impact Detection System (WLEIDS). It had been installed on all Space Shuttle missions till recent retirement of the fleet. The system tested accelerometers and AE sensors for detecting the impact of launch foam debris on the leading edge made of reinforced carbon-carbon and on thermal protection tiles. Even though a foam block tested was ~0.8 kg, its speed is 240-290 m/s and produced detectable damages with the sensors. Some hypervelocity (6.8 km/s) tests were done, indicating different waveforms from the slow impacts. Implementation on shuttle fleet relied on flight-qualified accelerometers that proved to function at lower frequency range than AE sensors, while reducing the signal acquisition frequency down to 20 kHz, beneficial in data

storage and transmission to the Mission Control on earth. For each Space Shuttle, 66 sensors were on board and 22 battery-powered data acquisition/wireless transmission units were mounted in each wing cavity. The system recorded data from all sensors continuously during launch and ascent to orbit. The data was transmitted wirelessly to a laptop computer in the crew compartment and then downlinked to ground. The monitored data consists of rms values of g-force. A summary file of the largest peaks is also stored and used for preliminary analysis. When warranted, detailed analysis follows. For all flights since Columbia, the WLEIDS has performed exceptionally well. None of probable impact events have been of amplitude consistent with critical damage to the RCC leading edge and in-flight inspection at the suspected impact locations using the Orbital Boom Sensing System has not revealed damage. Post-analysis of the entire records evaluated the system performance on flight for future deployment. Some of the waveform records in the ground tests can be seen in [161] and key components of the Shuttle Wing Leading Edge Impact Detection System are shown in Fig. 24.

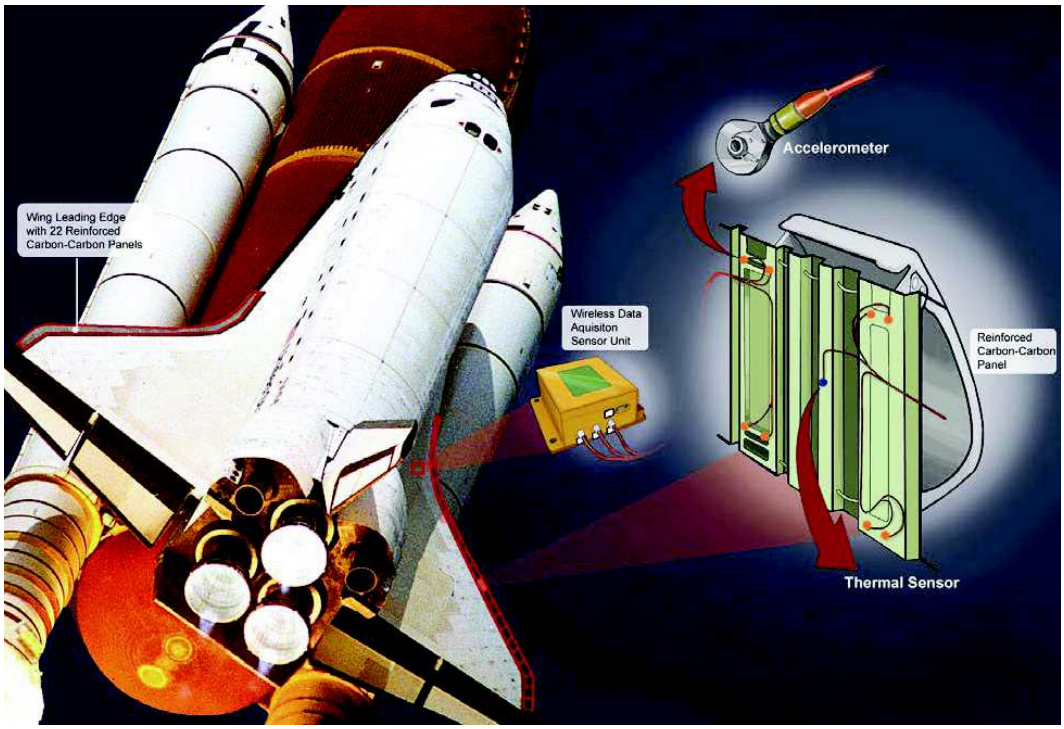

Fig. 24 Key components of the Shuttle Wing Leading Edge Impact Detection System. [161]

Sandwich structures

In practical composite design, sandwich structures are widely used [163]. Aluminum or Nomax honeycomb core is widely used in aerospace applications and foam core is common in less demanding design. AE studies of such structures are not many. Burman [164] conducted an extensive study of sandwich composites under static and fatigue loading conditions and used AE for monitoring crack initiation and growth in the core. AE location aided failure process study on invisible subsurface damages. AE behavior is typical one with rising AE near fracture, and amplitude reaching into >80-dB range. Sandwich composite panels are finding new applications in rehabilitating aging infrastructures [165, 166]. Reference [165] used a small AE system and obtained some AE results on tensile samples, but only rough data outline is given. Larger samples with cyclic loading are also tested, but results are not clearly analyzed or presented. [166] used 16-channel AE system and obtained some AE results during stepwise loading and signal attenuation on the panel, but definitive results are yet to come. In these ambitious projects, it is hoped that past AE experience in the literature is used to better outcomes.

In similar composites with 30+% GFRP skin and balsa-wood core, Hoa [167] studied their AE behavior extensively, producing an ASTM document (ASTM E1888-12). It is worth noting that, starting from FR concept, Hoa defined a trend number $Z = A_2/A_1$, where

A_1 is AE parameter (counts, hits) upon loading to P_1.

A_2 is AE parameter (counts, hits) upon reloading to P_1.

Under cyclic loads, Z tends to vanish in a good vessel (or a zone), while Z in damaged one starts to rise. This parameter is useful in judging this type of sandwich composite and may be applicable for other types.

Aircraft applications

In 1984, we were invited to monitor the testing of a prototype all Kevlar composite aircraft (Avtek) using AE. See Fig. 25, which shows an 8-channel AET-5000 system. The Avtek plane was supported at the main wings and canard wing tips while the mid-fuselage was pulled down. 30- and 175-kHz sensors were distributed, especially at the canard attachments. This position turned out to be much weaker than design load, producing significant AE and stopping the test before damage. This demonstrated the AE test's worth, but the Kevlar plane project did not continue long unfortunately.

Figure 25 AE monitoring of prototype Avtek aircraft in 1984. Dr. I. Roman, on leave from Hebrew University of Jerusalem, operated AET-5000 system. [The original of the cover photo shown in JAE vol. 3]

AE applications in aircraft industry appear to have advanced according to the anecdotes from AE equipment makers, but little is known in the open literature for obvious reason. Only about a dozen papers appeared in JAE in the past 30 years with direct connection to airframe, but only metallic. Composite structural components are increasing their importance even in commercial aircraft, but the role of AE is apparently limited. Pfeiffer and Wevers [168] detailed AE and Lamb wave methods for aircraft SHM applications as a part of AISHA project under European Research Area. For critical damages, appropriate Lamb modes are being identified for such parts as helicopter tailbooms and Airbus slat tracks. Takeda [169] reviewed small-diameter optical fiber sensors for damage monitoring and structural health monitoring (SHM) of composite structures. They also reported on results from ACS-SIDE project in Japan with optical SHM. Fiber-Bragg grating (FBG) sensors are combined with PZT actuators for Lamb wave inspection of CFRP structures. Several articles on NDT in aircraft manufacturing appeared recently [170-174], but only one briefly mentioned AE's use in predevelopment-design phase [170]. Our concerted efforts to change the perception of key people in this industry are needed. For example, an improved activation method of impact/delamination damage for AE diagnosis will be needed to provide a better technique to aircraft people. On composite panels, the benefit of global

inspection with AE often evaporates from high wave attenuation behavior. An innovative method is required also.

Figure 26 shows expanding uses of composite in modern commercial and military aircrafts. This poses a formidable challenge for NDE/NDT of composite components during manufacturing, service inspections, flight conditions and SHM. Numerous laboratory tests have been carried out during last decades on large composite components for aircraft structures. At the beginning of the 1990s, Boeing designed and built a 64-channels AE system, called AE Pre-failure Warning System (AEPWS), which was used on a prototype of a low tail horizontal stabilizer (LTHS) box [175]. AEPWS, based on calculation of the AE energy (MARSE), was used to monitor selected flights for the first lifetime (50,000 flights) of fatigue cycling of the LTHS. At the end of the 1990s, Saab Aerospace (Sweden) monitored by AE two full-scale test on the JAS 39 Gripen combat aircraft, partially manufactured from CFRP [176]. In the first one, the wings and the vertical stabilizer (which are primarily manufactured from CFRP) were monitored by a 72-channels PAC AE system in order to localize damage in the early stage. It was possible even without any false alarms and no more damage was detected by other NDT techniques. During the more than 100 real-time tests FR index was checked.

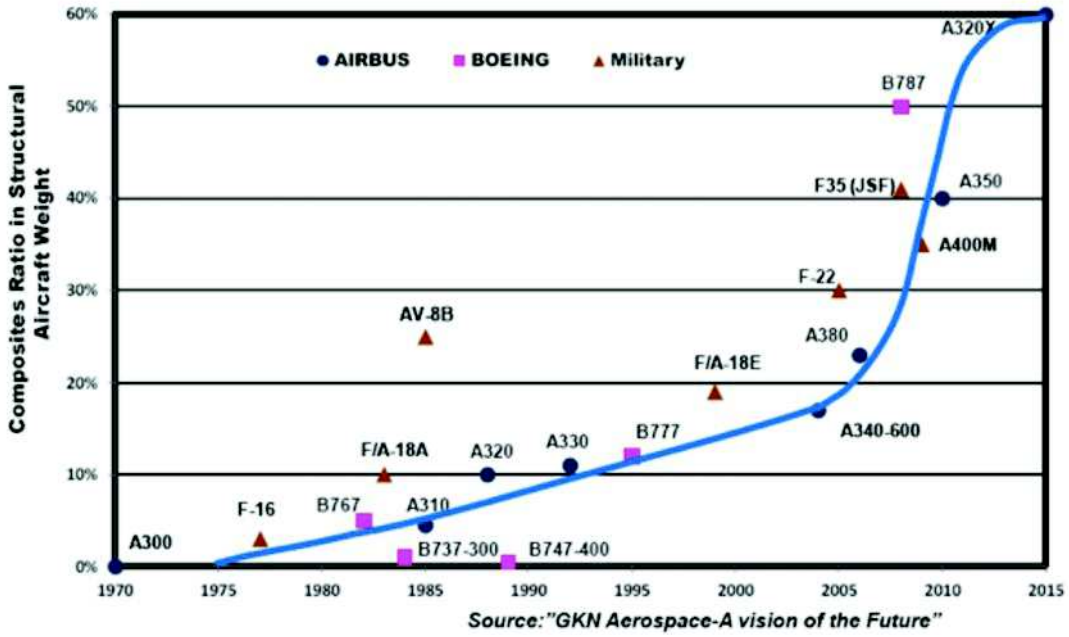

Fig. 26 Composites ratio in structural aircraft weight during last decades in commercial and military aircrafts.

Toward the goal of more active AE utilization in composite aircraft area, some papers are of interest [177-179]. Leone et al. [177] monitored AE in several honeycomb sandwich composites curved fuselage panes, each containing a different scenario of damage, using the Full Scale Aircraft Structure Test Evaluation and Research (FASTER) placed in Atlantic City (US). In particular, the evolution of particular notches artificially made on the full-scale T700-CFRP sandwich panels was monitored by AE using an 8-channel 150 kHz resonant sensor configuration located in circle (see Fig. 27). A good correlation was found between the notch progression (see Fig. 28) and AE accumulated and during loading of the panels (see Fig. 29). The most of the events recorded were below 70 dB (between 85-97 %). Figure 29 shows that the percentage of high-amplitude events, normally associated with fiber breakage, was less than 5% of the total AE events recorded.

Fig. 27 Left: Honeycomb sandwich composite panel. Right: A segment of the panel showing the AE sensors arrangement, a photogrammetry system and an artificial notch. [177]

Fig. 28 Notch-tip damage after complete final fracture in two sandwich panels. [177]

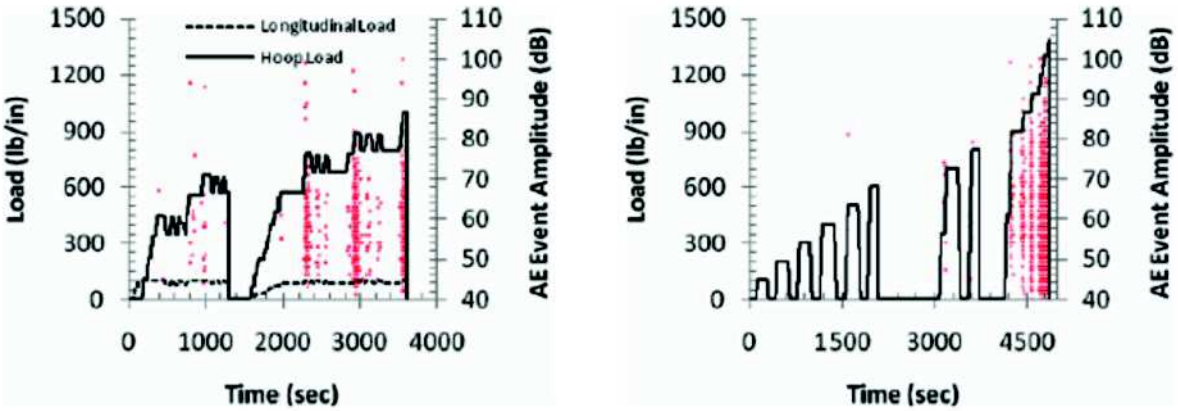

Fig. 29 Load-time history and accumulation of AE events and amplitudes recorded during loading two panels. Each dot signifies a three-hit event. [177]

Sensors and Sensing

Aljets [178, 179] completed a thesis with new approach to source location methods and validated them on large CFRP plates. One is to use an array of 3 closely positioned (45 mm) sensors. Using this sensor array, wave modes and source locations are obtained with two different methods. The array sensor approach is similar to Sachse's patent of 4-sensor array, but the latter was for source location purpose [180]. As we saw earlier in this review, the knowledge of wave modes is

very important information today. More such work on large samples must be pursued to make AE acceptable to industry engineers. In this connection, a new method of Lamb-wave detection should be of interest. Yeum et al. [181] used a sensor of two coaxial PZT elements, a center disc and a surrounding ring. This sensor needs to be placed only on one surface. The mode decomposition can be performed at any selected frequency without changing the PZT size and/or spacing configuration, aided by solving 3D Lamb-wave propagation equations with the PZT size and shape as input. This technique was demonstrated for Lamb waves in an aluminum plate, but should be applicable to composite plates as well.

Optical sensing of AE signals relied on bulky components initially, but the size of sensors and associated equipment started to shrink. Wevers et al. [182] introduced an intensity modulated optical sensor based on the microbending into a CFRP plate and evaluated AE from developing damage, though S/N ratio needed improvements. Surgeon and Wevers [183] evaluated effects of adding optical sensors into CFRP plates. When optical fibers are near the stress-carrying plies, degradation was detectable. Subsequent reports from this group [184, 185] examined signal processing aspect for S/N improvements and a different sensing principle, using polarimetric single-mode optical fiber sensors. Other approaches also appeared more recently [186-188] with interferometric techniques. FBG sensors are from a different principle and is amenable to source localization. See Tsuda's article [189] on its use in SHM applications along with [169]. For embedded usage, see [190]. The main obstacle for wider uses of optical sensing is still the cost of equipment.

Pattern recognition – Clustering

When we initiated using pattern recognition analysis (PRA) software, called ILS, in the early 1980s [61a, 191, 192], we relied on autoregressive modeling to obtain the signal feature vectors and utilized principal component analysis. It was cumbersome, but the promise of signal discrimination was encouraging. We next used Icepak software from TISEC in the 1990s, which vastly ran faster and reported CFRP signal classification results discussed earlier [61b,c, 95]. With Icepak, several algorithms including artificial neural network were available, but we primarily used k-NN. In these studies, we had to supply the likely clustering scheme based on separate aspects, such as special specimen geometry, loading range, microscopy, etc. Unsupervised PRA algorithm started to appear [193] and Noesis software improved the coordination with PAC's data acquisition hardware in an integrated operation. This approach basically uses the standard AE parameters along with partial power spectral density, chosen to represent different AE source features. A different approach is taken in Vallen's VisualClass that relies on time-staggered power spectral features. In the past decade, PRA has become a common tool in AE examination [194, 195; see also Hill, [23], pp. 382-387].

Kohonen introduced a new concept in classifying a large body of diverse data [196]. This is known as the Self-organizing Map (SOM). It has been incorporated into PRA scheme for AE data analysis [40, 82-85, 197-199]. For non-specialists, it is easiest to start with [40, 84]. In the simplest term, SOM helps achieve "Birds of a feather flock together" phenomenon by directing a data vector (characterized by multiple features) into an area of a map where other data vectors of similar characteristics are already present. Godin [84] combined SOM with k-means method to improve further AE data classification. [200, 201] are recent studies that take advantage of the new PRA method with SOM. SOM Toolbox for MATLAB is available from Prof. Kohonen's group [http://www.cis.hut.fi/somtoolbox/links/somsoftware.shtml] and can be incorporated into own data analysis package. With the SOM, robust unsupervised PRA is possible and this should become a practical AE analysis tool shortly.

Concluding Remarks

During the past ~50 years, we have expanded the knowledge base on AE. Still, further advances are critically needed to make AE an indispensable tool for composite industry. This article has attempted to review "composite AE" from materials researchers' perspectives and to survey how AE has contributed to various applications. The first part was reasonably achieved but the second part was only partially fulfilled, as it has been difficult to gain information of AE technology practiced in various industries. We have also identified a few crucial problems that have to be resolved to reach our goal of making AE a useful tool for industry. These include displacement-velocity sensor response, high wave attenuation in composites and the lack of understanding of Felicity effect and stress rupture. Promising developments include new methods for high-pressure vessel monitoring sanctioned by ASME, SOM-based unsupervised PRA, and tackling of issues with wave attenuation and stress rupture. We trust this article presents a fresh summary of what has been discovered and utilized, points out obstacles to surmount and gives some suggestions to future work, hopefully serving as inspiration for developing a new technology.

Acknowledgment: The author (K.O.) wishes to thank Drs. Timothy Fowler and Michael Gorman for critically reviewing this manuscript.

References

1. a) A.T. Green, C.S. Lockman, R.K. Steele, Acoustic verification of structural integrity of Polaris chambers, Modern Plastics, vol. 41, July 1964, pp. 137-139, 178, 180.
b) A.T. Green, C.S. Lockman, H.K. Haines, Acoustical analysis of filament-wound Polaris chambers, Report 0672-01F. Aerojet-General Corporation, Sacramento, CA. [NTIS: AD418330] 1963.
2. a) A.T. Green, C.S. Lockman, S.J. Brown, R.K. Steele, "Feasibility study of acoustic repressurization system," NASA CR55472, March 1966.
b) A.T. Green, Proc. 27th European Conference on Acoustic Emission Testing (EWGAE27), Cardiff, Wales, UK, Sep. 2006, pp. 3-16.
3. T. Asakawa and C.F. Peregoy, "Manufacturing technology for large monolithic fiberglass reinforced plastic rocket motor case", Volume I, II. Appendixes. DTIC AD0483226, Nov. 1965.
4. E.C. Jenssen, H. Spanheimer, A.J. De Herrera, "Prediction of composite pressure vessel performance by application of the Kaiser effect in acoustic emissions", Presented at the American Society of Mechanical Engineers, Paper No. H300-12-2-037, June 1975.
5. R.G. Liptai, "Acoustic emission from composite materials," *Composite Materials: Testing and Design*, ASTM-STP-497, 1972, pp. 285-298.
6. a) H.C. Kim, A.P. Ripper Neto and R.W.B. Stephens, "Some observations on acoustic emission during continuous tensile cycling of a carbon fibre/epoxy composite," Nature, Physical Science, vol. 237, 1972, pp. 78-80.
b) M. Takehana and I. Kimpara, "AE from FRP fracture processes," *Proc. US-Japan Symposium on Acoustic Emission, Japanese volume*, 1972, Sec. 4, pp. 1-22.
7. J. Fitz-Randolph, D.C. Phillips, P.W.R. Beaumont and A.S. Tetelman, "Acoustic emission studies of a boron-epoxy composite", J. Comp. Matls, vol. 5, 1971, pp. 542-548.
8. T.J. Fowler, "Acoustic Emission Testing of Fiber Reinforced Plastics" American Society of Civil Engineers (ASCE) Fall Convention and Exhibit, Preprint 3092, ASCE, New York, 1977.
9. T.J. Fowler (1979), "Acoustic Emission Testing of Fiber Reinforced Plastics," Proceedings Paper 15021, J. Technical Council, ASCE, vol. 105 (TC2): 281-289.

10. T.J. Fowler and E. Gray (1979), "Development of an Acoustic Emission Test for FRP Equipment." Preprint 3583, American Society of Civil Engineers, New York, 1979.
11. T.J. Fowler and R.S. Scarpellini (1980), "Acoustic Emission Testing of FRP Equipment - I," Chemical Engineering, CHEEA, vol. 87, no. 21: 145-148.
12. T.J. Fowler, "Acoustic emission testing of chemical process industry vessels," *Progress in Acoustic Emission II* (Proc. IAES-7), JSNDI, Tokyo, 1984, pp. 421-449.
13. T.N. Crump and M.A. Droge, "The Characterization of Fiberglass Reinforced Plastics Using Acoustic Emission", Managing Corrosion with Plastics, Volume IV, National Association of Corrosion Engineers, 1979, Houston.
14. T.G. Hagemeier, "Monitoring of an FRP Pressure Vessel During Pressure Testing", Managing Corrosion with Plastics, Volume IV, National Association of Corrosion Engineers, 1979, Houston.
15. CARP, "Recommended Practice For Acoustic Emission Testing of Fiberglass Reinforced Plastic Resin (RP) Tanks/Vessels", The Society of the Plastics Industry, Inc., New York, 1982, 13 p. Revised and republished, 1987.
16. a) ASME, "Acoustic emission examination of fiber reinforced plastic vessels", Boiler and Pressure Vessel Code, Section V, Article 11, Nondestructive Examination, American Society of Mechanical Engineers, New York, 1985, 2010.
b) ASTM E1067/E1067M-11 Standard Practice for Acoustic Emission Examination of Fiberglass Reinforced Plastic Resin (FRP) Tanks/Vessels, 2011.
17. T.F. Fowler, "Revisions to the CARP Recommended Practice for Tanks and Vessels", Proc. AECM-5, 1995, pp. 263-272.
18. P.H. Ziehl, "Development of a damage based design criterion for fiber reinforced vessels", PhD Thesis, The University of Texas at Austin, 2000, 317 p.
19. N. Ativitavas, "Acoustic emission signature analysis of failure mechanisms in fiber reinforced plastic structures", PhD Thesis, The University of Texas at Austin, 2002, 444 p.
20. T.J. Fowler, "Experience with acoustic emission monitoring of chemical process industry vessels," *Progress in Acoustic Emission III* (Proc. IAES-8), JSNDI, Tokyo, 1986, pp. 150-162.
21. R. Davies, "Acoustic emission as a basis for plant integrity monitoring", *Progress in Acoustic Emission III* (Proc. IAES-8), JSNDI, Tokyo, 1986, pp. 9-25.
22. T.J. Fowler, J.A. Blessing, P.J. Conlisk and T.L. Swanson, The MONPAC system, J. Acoustic Emission, vol. 8, no. 3, 1989, 1-10.
23. *Acoustic Emission Testing, Nondestructive Testing Handbook*, 3rd edition, Vol. 6, American Society for Nondestructive Testing, Columbus, OH, 2005. (2nd edition, Vol. 5, 1987).
24. a)-f) *Proceedings of 1st to 6th International Symp. on AE from Reinforced Plastics/Composite Materials*, SPI/ASNT, 1983, 1986, 1989, 1992, 1995, 1998.
25. M.A. Hamstad, "A review: acoustic emission as a tool for composite materials studies," Experimental Mechanics, vol. 26, no. 1, March 1986, pp. 7-13.
26. M. A. Hamstad, "Thirty years of advances and some remaining challenges in the application of acoustic emission to composite materials," *Acoustic Emission Beyond the Millennium*, eds. T. Kishi et al., Elsevier, Oxford, UK, 2000, pp. 77-91.
27. CARP Aerospace/Advanced composites subcommittee. "Guidance for development of AE applications on composites", J. Acoustic Emission, vol. 11, 1993, *pp.* C1–C24.
28. J. Bohse, "Acoustic emission examination of polymer–matrix composites", J. Acoust Emission, vol. 22, 2004, pp. 208–23.
29. M.R. Gorman, "Acoustic emission in structural health monitoring (SHM)", *Encyclopedia of Structural Health Monitoring*, ch. 4, eds. C. Boller et al., J. Wiley, 2009, pp. 79-100.
30. K. Lambrighs, M. Wevers, "Applications of acoustic emission for SHM: A review", *Encyclopedia of Structural Health Monitoring*, ch. 13, eds. C. Boller et al., J. Wiley, 2009, pp. 289-

301.
31. K. Ono, “Acoustic Emission in Materials Research – A Review”, J. Acoust Emission, vol. 29, 2011, pp. 284–308.
32. T.F. Drouillard, M.A. Hamstad, ref. 24a, sec. 6, pp. 1-60; 24b, pp. 60-71, 24c, pp. 391-413.
33. J. Wolters, “Acoustic emission monitoring of fracture mechanisms in short fiber reinforced thermoplastics: basic studies on model compounds”, ref. 24b, pp. 29-36, 1986.
34. L. Lorenzo and H.T. Hahn, “Acoustic emission study of fracture of fibers embedded in epoxy matrix”, ref. 24a, session 2, pp. 1-13, 1983.
35. T. Imafuku, M. Shiwa, N. Koizumi, S. Yuyama, and T. Kishi, “Acoustic emission testing of FRP panel tank”, ref. 24b, pp. 180-183, 1986.
36. I. Roman and K. Ono, "Acoustic emission characterization of fracture mechanisms in woven roving glass-epoxy composites," *Progress in Acoustic Emission, II*, eds. M. Onoe et al., JSNDI, Tokyo, 1984, pp. 496-503.
37. N.V. De Carvalho, S.T. Pinho, P. Robinson, “An experimental study of failure initiation and propagation in 2D woven composites under compression”, Composites Science and Technology, vol. 71, 2011, pp. 1316–1325.
38. R.A. Nordstrom, “Acoustic emission characterization of microstructural failure in the single fiber fragmentation test”, PhD. Thesis, Swiss Federal Institute of Technology, Diss. No. 11402, Zurich, Switzerland, 1996.
39. J. Bohse, “Acoustic emission characteristics of micro-failure process in polymer blends and composites, Compos Sci Technol. vol. 60, 2000, 1213–1226.
40. R. de Oliveira (R.F.da C. Oliveira), “*Health Monitoring of FRP using Acoustic Emission and Fibre Optic Techniques*”, PhD Thesis, University of Porto, 2004, 237 p.
41. M. R’Mili, M. Moevus, N. Godin, “Statistical fracture of E-glass fibres using a bundle tensile test and acoustic emission monitoring”, Compos Sci Technol. vol. 68, 2008, 1800–1808.
42. L. Lorenzo, H.T. Hahn, “On the applicability of amplitude distribution analysis to the fracture process of composite materials”, J. Acoustic Emission, vol. 5, 1986, pp. 15-24.
43. S.A. Carey, “Acoustic emission and acousto-ultrasonic signature analysis of failure mechanisms in carbon fiber reinforced polymer materials”, PhD Thesis, 2008, College of Engineering and Computing, University of South Carolina, Columbia, SC.
44. A. Nanjyo, M. Mohri, K. Ono, “Acoustic emission behavior during tensile fracture of resin-impregnated strands of pitch-based carbon fiber”, ref. 24d, pp. 44-54, 1992.
45. J.M. Berthelot, J. Rhazi, “Different types of amplitude distributions in composite materials”, ref. 24b, 1986, pp. 96-103.
46. J.M. Berthelot, J. Rhazi, “Acoustic emission in carbon fibre composites”, Composites Science and Technology, vol. 37, 1990, 411-428.
47. D. Valentin, Ph. Bonniau, A.R. Bunsell, ”Failure mechanism discrimination in carbon fibre-reinforced epoxy composites”, Composites, vol. 14, 1983, pp. 345-351.
48. K. Ono, “Acoustic emission behavior of flawed unidirectional carbon fiber-epoxy composites”, J. of Reinforced Plastics and Composites, Vol. 7, January 1988, pp. 90-105.
49. See also ref. 24b, pp. 22-28. Table 2 was not printed correctly in ref. 48a above.
50. J. Awerbuch, M. R. Gorman and M. Madhukar, “Monitoring damage accumulation in filament-wound graphite/epoxy laminate coupons during fatigue loading through acoustic emission”, ref. 24a, 1983, pp. 73-102.
51. a) P. Wright, M. Mavrogordato, A.J. Moffat, I. Sinclair, S.M. Spearing, “High resolution computed tomography for modelling laminate damage”, Proc 17th Int Conf Compos Mater., ICCM-17, Edinburgh, 2009, paper T1.4, 10 p.
http://www.iccm-central.org/Proceedings/ ICCM17proceedings/Themes/TSAI/T1.4%20Wright.pdf
52. A.E. Scott, M. Mavrogordato, P. Wright, I. Sinclair, S.M. Spearing, “In situ fibre fracture

measurement in carbon–epoxy laminates using high resolution computed tomography", Compos Sci Technol. vol. 71, 2011, pp. 1471–1477.
53. M.G.R. Sause, T. Müller, A. Horoschenkoff and S. Horn, "Quantification of failure mechanisms in mode-I loading of fiber reinforced plastics utilizing acoustic emission analysis", Composites Science and Technology, vol. 72, 2012, pp. 167–174
54. K. Ono, "Acoustic emission behavior of metal-fiber laminates", *Progress in Acoustic Emission XIV*, IAES19, JSNDI, 2008, pp. 201-208.
55. A.R.A. Abraham, K.L. Johnson, C.T. Nichols, R.L. Saulsberry, J.M. Waller, "Use of statistical analysis of acoustic emission data on carbon-epoxy COPV materials-of-construction for enhanced felicity ratio onset determination", NASA report JSC-CN-26080, pp. 1-15, 2012.
56. J.M. Waller, R.L. Saulsberry and E. Andrade, "Use of acoustic emission to monitor progressive damage accumulation in Kevlar®-49 composites," *QNDE Conference vol. 29*. AIP Conf. 1211, 2010, pp. 1111-1118.
57. P.D. Washabaugh, W.G. Knauss, "A reconciliation of dynamic crack velocity and Rayleigh wave speed in isotropic brittle solids", Intl J. of Fracture, vol. 65, 1994, pp. 97-114.
58. T. Cramer**,** A. Wanner, and P. Gumbsch, "Crack velocities during dynamic fracture of glass and single crystalline silicon, phys. stat. sol. (a), vol. 164, 1997, pp. R5-R6.
59. M.R. Gorman, "Modal AE analysis of fracture and failure in composite materials, and the quality and life of high pressure composite pressure vessels", J. Acoustic Emission, vol. 29, 2011, pp. 1-28.
60. B.W. Kim, J.A. Nairn, "Observations of fiber fracture and interfacial debonding phenomena using the fragmentation test in single fiber composites", J. Composite Mat., vol. 36, no. 15, 2002, pp. 1825-1858.
61. a) M. Ohtsu and K. Ono, "Pattern recognition analysis of acoustic emission from unidirectional carbon fiber-epoxy composites by using autoregressive modeling," J. Acoustic Emission, vol. 6, 1987, pp. 61-72.
b) Q. Huang, Characterization of acoustic emission from failure processes of carbon fiber/epoxy composites by pattern recognition", PhD thesis, University of California, Los Angeles, 1993, 172 p.
c) K. Ono and Q. Huang, "Pattern recognition analysis of acoustic emission signals", *Progress in Acoustic Emission VII*, eds. T. Kishi et al., JSNDI, Tokyo, 1994, pp. 69-78.
62. K. Ono, H. Cho and T. Matsuo, "Experimental transfer functions of acoustic emission sensors", J. of Acoustic Emission, vol. 26, 2008, pp. 72-90.
63. A. Maslouhi. C. Roy and D. Proulx, "Characterization of acoustic emission signals generated in carbone-epoxy composites", ref 24b, pp. 112-116, 1986.
64. P.J. de Groot, P.A.M. Wijnen, R.B.F. Janssen, "Real-time frequency determination of acoustic emission for different fracture mechanisms in carbon/epoxy composites", Composites Science and Technology, vol. 55, 1995, pp. 405-412.
65. M. Giordano, A. Calabro, C. Esposito, A. Lizza, A. D'Amore, L. Nicolais, "An acoustic emission characterization of the failure modes in polymer-composite materials", Composite Science and Technology, vol. 58, 1997, pp. 1923-1928
66. M. Eaton, K. Holford, C. Featherston, R. Pullin, "Damage in carbon fibre composites: the discrimination of acoustic emission signals using frequency", J Acoust Emission vol. 25, 2007, pp. 140–8.
67. a) C.B. Scruby, "Acoustic emission measurements using point-contact transducers," J. of Acoustic Emission, vol. 4, 1985, pp. 9-18.
b) D.J. Buttle, C.B. Scruby, "Characterization of fatigue of aluminum alloys by acoustic emission, Part I and II, J. Acoustic Emission, vol. 9, 1990, pp. 243-254, 255-270.
68. D. Guo, A. Mal and K. Ono, "Wave theory of acoustic emission in composite laminates", J. of Acoustic Emission, vol. 14, 1996, pp. S19-S46.

69. M.G.R. Sause and S. Horn, “Simulation of lamb wave excitation for different elastic properties and acoustic emission source geometries”, J. Acoustic Emission, vol. 28, 2010, pp. 142-154.
70. M. Sause, “Identification of failure mechanisms in hybrid materials utilizing pattern recognition techniques applied to acoustic emission signals”, Augsburg Univ. doctoral dissertation, Mensch und Buch Verlag, 2010, 305 p.
71. a) H. Suzuki, M. Takemoto and K. Ono, “The fracture dynamics in a dissipative glass-fiber/epoxy model composite with AE source simulation analysis”, J. Acoustic Emission, vol. 14, 1996, pp. 35-50.
b) H. Suzuki, “Fracture dynamics via inverse analysis of viscoelastic waves”, doctoral thesis, Tokyo Inst. Technology, 2000, 176 p.
72. e.g., M. Enoki, T. Kishi, “Acoustic emission source characterization in materials”, *Acoustic Emission – Beyond the Millenium*, 2000, Elsevier, pp. 1-17.
73. R.L. Weaver, W. Sachse and L. Niu, "Transient ultrasonic waves in a viscoelastic plate: Theory", J. Acoust. Soc. Am., vol. 85, no. 6, 1989, pp. 2255-2261.
74. M. Ohtsu and K. Ono, "A generalized theory of acoustic emission and Green's function in a half space", J. Acoustic Emission, vol. 3, no. 1, 1984, pp. 27-40.
75. J.M. Berthelot, “Relation between amplitudes and rupture mechanisms in composite materials”, ref. 24b, 1986, pp. 126-133.
76. J.E. Bailey, P.T. Curtis and A. Parvizi, “On the Transverse Cracking and Longitudinal Splitting Behaviour of Glass and Carbon Fibre Reinforced Epoxy Cross Ply Laminates and the Effect of Poisson and Thermally Generated Strain”, Proc. R. Soc. Lond. A vol. 366, 1979, pp. 599-623.
77. a) W.H. Prosser, “Advanced AE techniques in composite materials research”, J. Acoustic Emission, vol. 14, 1996, pp. S1-S11.
b) M.R. Gorman and S. M. Ziola, "Plate waves produced by transverse matrix cracking," Ultrasonics, vol. 29, 1991, pp. 245-251.
78. S.-C. Woo, N.-S. Choi, “Analysis of fracture process in single-edge-notched laminated composites based on the high amplitude acoustic emission events”, Composites Science and Technology, vol. 67, 2007, pp. 1451–1458.
79. M. Schoßig, A. Zankel, C. Bierögel, P. Pölt, W. Grellmann, “ESEM investigations for assessment of damage kinetics of short glass fibre reinforced thermoplastics – Results of in situ tensile tests coupled with acoustic emission analysis”, Composites Science and Technology, vol. 71, 2011, pp. 257–265.
80. A. Bussiba, M. Kupiec, S. Ifergane, R. Piat, T. Böhlke, “Damage evolution and fracture events sequence in various composites by acoustic emission“, Science and Technology, vol. 68, 2008, pp. 1144-1155.
81. P.L. Chiou, W.L. Bradley, “Moisture-induced degradation of glass/epoxy filament-wound composite tubes”, J. of Thermoplastic Composite Materials, vol. 9, no. 2, 1996, p. 118.
82. S. Huguet, N. Godin, R. Gaertner, L. Salmon, D. Villard, “Use of acoustic emission to identify damage modes in glass fibre reinforced polyester”, Composites Science and Technology, vol. 62, 2002, pp. 1433–1444.
83. N. Godin, S. Huguet, R. Gaertner, L. Salmon, “Clustering of acoustic emission signals collected during tensile tests on unidirectional glass/polyester composite using supervised and unsupervised classifiers”, NDT&E International, vol. 37, 2004, pp. 253–264.
84. N. Godin, S. Huguet, R. Gaertner, “Integration of the Kohonen’s self-organising map and k-means algorithm for the segmentation of the AE data collected during tensile tests on cross-ply composites”, NDT&E International, vol. 38, 2005, pp. 299–309
85. N. Godin, S. Huguet, R. Gaertner, “Influence of hydrolytic ageing on the acoustic emission signatures of damage mechanisms occurring during tensile tests on a polyester composite: Application of a Kohonen’s map”, Composite Structures, vol. 72, 2006, pp. 79-85.

86. L. Lagunegrand, T. Lorriot, R. Harry, H. Wargnier, J.M. Quenisset, “Initiation of free-edge delamination in composite laminates”, Composites Science and Technology, vol. 66, 2006, pp. 1315–1327.
87. J.J. Scholey, P.D. Wilcox, M.R. Wisnom and M.I. Friswell "Quantitative experimental measurements of matrix cracking and delamination using acoustic emission," Composites: Part A, vol. 41, 2010, pp. 612-623.
88. J. Bohse, T. Krietsch, J.H. Chen, A.J. Brunner, “Acoustic emission analysis and micromechanical interpretation of mode I fracture toughness test on composite materials”, Fracture of polymers, composites and adhesives, eds. J.G. Williams and A. Pavan, ESIS publication 27, 2000, pp. 15 – 26.
89. J. Bohse, J. Chen, Acoustic emission examination of mode I, mode II and mixed mode I/II interlaminar fracture of unidirectional fiber-reinforced polymers. J. Acoust Emission, vol. 19, 2001, pp. 1–10.
90. W. Mielke, A. Hampe, O. Hoyer, K. Schumacher, “Analysis of AE-events from single fibre pull-out experiments, ref. 24c, 1989, pp. 323-331; see also J. Acoust Emission, vol. 9, 1990, pp. 103-108.
91. M. Enoki, D. Valentin, H. Tsuda & T. Kishi, “Characterization of debonding process of fiber reinforced composites by acoustic emission”, Nondestructive Testing and Evaluation, vol. 8-9, 1992, pp. 857-868.
92. K. Tanaka, K. Minoshima, W. Grela, K. Komai, “Characterization of the aramid/epoxy interfacial properties by means of pull-out test and influence of water absorption”, Composites Science and Technology, vol. 62, 2002, pp. 2169–2177.
93. Y. Mizutani, K. Nagashima, M. Takemoto, K. Ono, “Fracture mechanism characterization of cross-ply carbon-fiber composites using acoustic emission analysis”, NDT&E International, vol. 33, 2000, pp. 101-110.
94. K. Ono, Y. Mizutani, M. Takemoto, “Analysis of acoustic emission from impact and fracture of CFRP laminates,” J. Acoustic Emission, vol. 25, 2007, pp. 179-186.
95. K. Ono, Q. Huang, J.Y. Wu, “AE pattern recognition analysis of the fracture of glass fiber composites exposed to hot-wet conditions”, ref. 24e, 1995, pp. 197-204.
96. M.A. Hamstad, “A discussion of the basic understanding of the Felicity effect in fiber composites”, J. Acoustic Emission, vol. 5, 1986, pp. 95-102.
97. J. Awerbuch, M. R. Gorman and M. Madhukar, “Monitoring acoustic emission during quasi-static loading/unloading cycles of filament-wound graphite/epoxy laminate coupons”, ref. 24a, 1983, pp. 139-157.
98. Z. Yuan, “Acoustic emission characterizations of internal damage for GFRP”, *Progress in Acoustic Emission II* (Proc. IAES-7), JSNDI, Tokyo, 1984, pp. 458-463.
99. O.-Y. Kwon and D.-H. Hong, Acoustic emission monitoring of impact-damaged CFRP laminates during flexural tests”, *Progress In Acoustic Emission VIII*, JSNDI, 1996, pp. 163-168.
100. J.-H. Shin, O.-Y. Kwon , “Acoustic emission monitoring of lightning-damaged CFRP laminates during compression-after-impact test”, J. Korean Society for Nondestructive Testing, vol. 32, no. 3, 2012, pp. 269-275.
101. F. Lachaud, B. Lorrain, L. Michel, R. Barriol, “Experimental and numerical study of delamination caused by local buckling of thermoplastic and thermoset composites”, Composites Science and Technology, vol. 58, 1998, pp. 721-733
102. R.L. Saulsberry, N.J. Greene, L. Hernandez, “Stress rupture nondestructive evaluation of composite overwrapped pressure vessels”.
http://research.jsc.nasa.gov/BiennialResearchReport/2011/287-2011-Biennial.pdf

103. J.M. Waller, C.T. Nichols, D.J. Wentzel, and R.L. Saulsberry, “Use of modal acoustic emission to monitor damage progression in carbon fiber/epoxy composites”, QNDE Conference, vol. 30, AIP Conf. 1335, 919-926, 2011.
104. J.M. Waller, R.L. Saulsberry, E. Andrade, “Use of acoustic emission to monitor progressive damage accumulation in Kevlar 49 composites”, QNDE Conference, vol. 29, AIP Conf. 1211, 2010, pp. 1111-1118.
105. NASA - NNWG NDE Working Group Homepage, updated April 10, 2012.
http://www.nnwg.org/current/WSTF/In-Situ NDE.html
106. K. Naito, Y. Tanaka, J.-M. Yang, Y. Kagawa, “Tensile properties of ultrahigh strength PAN-based, ultrahigh modulus pitch-based and high ductility pitch-based carbon fibers”, Carbon, vol. 46, 2008, pp. 189–195.
107. K.F. Graff, *Wave Motion in Elastic Solids*, Oxford, 1975, 649 p.
108. M.R. Gorman and W.H. Prosser, "AE source orientation by plate wave analysis," J. Acoustic Emission, vol. 9, no. 4, 1990, pp. 283-288.
109. M.R. Gorman and S. M. Ziola (1991), "Plate waves produced by transverse matrix cracking," Ultrasonics, vol. 29, 1991, pp. 245-251.
110. M.R. Gorman (1991), "Plate wave acoustic emission," J. Acoustical Society of America, vol. 90, no. 1, 1991, pp. 358-364.
111. J. Gary and M. Hamstad, "On the far-field structure of waves generated by a pencil break on a thin plate," J. Acoustic Emission, vol. 12, no. 3-4, 1994, pp. 157-170.
112. M.A. Hamstad, J. Gary, A. O'Gallagher, "Far-field acoustic emission waves by three-dimensional finite element modeling of pencil breaks on a thick plate," J. Acoustic Emission, vol. 14, no. 2, 1996, pp. 103-114.
113. M.A. Hamstad, J. Gary, A. O'Gallagher, "Wideband acoustic emission signals as a function of source rise-time and plate thickness," J. Acoustic Emission, vol. 16, 1998, pp. S251-S259.
114. W.H. Prosser, M.A. Hamstad, J. Gary, A. O'Gallagher, "Comparison of finite element and plate theory methods for modeling acoustic emission waveforms," J. of Nondestructive Evaluation, vol. 18, no. 3, 1999, pp. 83-90.
115. K.S. Downs and M.A. Hamstad, "Correlation of regions of acoustic emission activity with burst locations for spherical graphite/epoxy pressure vessels," J. Acoustic Emission, vol. 13, nos. 3-4, 1995, pp. 56-66.
116. A.K. Mal, Y. Bar-Cohen and S.S. Lih, "Wave attenuation in fiber-reinforced composites," M3D: *Mechanics and Mechanisms of Material Damping*, ASTM STP 1169, American Society for Testing and Materials, 1992, pp. 245-261.
117. M. Castaings, B. Hosten, “Air-coupled measurement of plane wave, ultrasonic plate transmission for characterising anisotropic, viscoelastic materials”, Ultrasonics, vol. 38, 2000, pp. 781–786.
118. M. Castaings, B. Hosten, T. Kundu, “Inversion of ultrasonic, plane-wave transmission data in composite plates to infer viscoelastic material properties. NDT & E International, vol. 33, no.6, 2000, pp. 377–92.
119. B. Hosten, “Heterogeneous structure of modes and Kramers–Kronig relationship in anisotropic viscoelastic materials”, J. Acoust. Soc. Am. vol. 104, no. 3, September 1998, pp. 1382-1388.
120. M. Castaings, M.V. Predoi, B. Hosten, “Ultrasound propagation in viscoelastic material guides”, *Proceedings of the COMSOL Multiphysics User's Conference 2005 Paris*, 6 p.
121. M. Calomfirescu, “Lamb Waves for Structural Health Monitoring in Viscoelastic Composite Materials”, Logos Verlag, Berlin, Germany, 2008. 119 p.
122. M.A. Torres-Arredondo, C.-P. Fritzen, “A viscoelastic plate theory for the fast modelling of Lamb wave solutions in NDT/SHM applications”, Ultragarsas (Ultrasound), vol. 66, no. 2, 2011,

pp. 7-13.
123. L. Wang, F.G. Yuan, “Group velocity and characteristic wave curves of Lamb waves in composites: Modeling and experiments”, Composites Science and Technology, vol. 67, 2007, pp. 1370–1384.
124. M.D. Seale and B.T. Smith, “Lamb wave propagation in thermally damaged composites”, *Review of Progress in QNDE*, eds. D.O. Thompson and D.E. Chimenti, vol. 15A, Plenum Press, New York, 1996, pp. 261-266.
125. G. Caprino, V. Lopresto, C. Leone, I. Papa, “Acoustic emission source location in unidirectional carbon-fiber-reinforced plastic plates with virtually trained artificial neural networks”, J. of Applied Polymer Science, vol. 122, 2011, pp. 3506–3513.
126. L. Taupin, A. Lhémery and G Inquiété, “A detailed study of guided wave propagation in a viscoelastic multilayered anisotropic plate”, J. Phys.: Conf. Ser. vol. 269, 2011, 012002, 14 p.
127. A. Gallego and K. Ono, “An improved acousto-ultrasonic scheme with lamb wave mode separation and damping factor in CFRP plates”, *Proc. EWGAE30-ICAE7*, Granada, Spain, 2012, pp. 573-580.
128. R. Joselin, T. Chelladurai, “Burst pressure prediction of composite pressure chambers using acoustic emission technique: a review”, J. Fail. Anal. and Preven. vol. 11, 2011, pp. 344–356.
129. J.W. Whittaker, W.D. Brosey and M.A. Hamstad, “Felicity ratio behavior of pneumatically and hydraulically loaded spherical composite test specimens”, J. Acoustic Emission, vol. 9, 1990, pp. 75-83
130. J.W. Whittaker, W.D. Brosey and M.A. Hamstad, “Correlation of Felicity ratio and strength behavior of impact-damaged spherical composite test specimens”, J. Acoustic Emission, vol. 9, 1990, pp. 84-90
131. M.R. Gorman, “Burst prediction by acoustic emission in filament wound pressure vessels”, J. Acoustic Emission, vol. 9, 1990, 131-139.
132. K.S. Downs and M.A. Hamstad, "Correlation of acoustic emission Felicity ratios and hold-based rate movement and burst strength," J. Acoustic Emission, vol. 13, nos. 3-4, 1995, pp. 45-55.
133. K.S. Downs and M.A. Hamstad, "Acoustic emission from depressurization to detect/ evaluate significance of impact damage to graphite/epoxy pressure vessels," J. Composite Materials, vol. 32, no. 3, 1998, pp. 258-307.
134. Y. Mizutani, K. Saiga, H. Nakamura, N. Takizawa, T. Arakawa and A. Todoroki, “Integrity evaluation of COPVs by means of acoustic emission testing”, J. Acoustic Emission, vol. 26, 2008, pp. 109-119.
135. Y. Mizutani, S. Sugimoto, R. Matsuzaki, A. Todoroki, “Fundamental study on integrity evaluation method for COPVs by means of acoustic emission testing”, J. Acoustic Emission, vol. 27, 2009, pp. 89-97.
136. J.B. Chang, “Implementation guidelines for ANSI/AIAA S-081: Space systems composite overwrapped pressure vessels”, *Aerospace Report No. TR-2003(8504)-1*, AD A413531, 2003, 83 p.
137. M.A. Hamstad and T.T. Chiao, "Acoustic emission from stress rupture and fatigue on an organic fiber composite," *Composite Reliability*, ASTM STP 580, 1975, pp. 191-201, UCRL-74745.
138. C. Le Floc, “Acoustic emission applied to observe damage in composite material high-pressure fluid storage tanks”, Societe Nationale Industrielle Aerospatiale Paris (France), ESA-86-97173, AD-D440906, 1986.
139. P.L. Chiou, W.L. Bradley, “Moisture-induced degradation of glass/epoxy filament-wound composite tubes”, J. of Thermoplastic Composite Materials, vol. 9, no. 2, 1996, p. 118.
140. M.R. Horne, E.I. Madaras, “Evaluation of acoustic emission NDE of Kevlar composite over

wrapped pressure vessels", NASA/TM-2008-215558, Langley Research Center, Hampton, Virginia, 2008.
141. W.W. Schmidt, G.M. Ecord, "Static fatigue life of Kevlar aramid/epoxy pressure vessels at room and elevated temperatures", NASA Johnson Space Center, AD-D437607, AIAA PAPER 83-1328, 1983.
142. E.Y. Robinson, "Design prediction for long term stress rupture service of composite pressure vessels", NASA_Techdoc_19950021870, Accession-ID: 95N28291, 1995.
143. G.M. Fallatah, N. Dodds and A.G. Gibson, "Long term creep and stress rupture of aramid fibre", Plastics, Rubber and Composites, vol. 36, no. 9, 2007, pp. 403-412.
144. M.T. Kezirian, K.L. Johnson, S.L. Phoenix, "Composite overwrapped pressure vessels (COPV): Flight rationale for the Space Shuttle Program", AIAA Paper, 2011.
http://ntrs.nasa.gov/archive/nasa/casi.ntrs.../20110015972_2011016890.pdf
145. D. McColskey, M. Hamstad, R. Saulsberry, J. Waller, "Production/performance monitoring of composite tanks nde methods for certification and production/performance monitoring of composite tanks", NIST-NASA presentation.
http://www1.eere.energy.gov/hydrogenandfuelcells/pdfs/ihfpv_mccloseky.pdf
146. J. Bohse. G.W. Mair and P. Novak, "Acoustic emission testing of high-pressure composite cylinders", EWGAE27, 2006, 267-272.
147. P. Tscheliesnig, "More than a quarter century of acoustic emission testing (AT) at TÜV Austria", EWGAE27, 2006, pp. 365-376.
148. G. Lackner, R. Dusek, A case study for crack detection within a gas cylinder using acoustic emission testing", EWGAE29, 2010, pp. 224-230.
149. D.R. Stephens and R.L. Osborne (Battelle), "Composite propane cylinder regulatory approval request", Docket 10662, Propane Education & Research Council, Washington DC, 2004.
150. Anon. *FRP Inspection Guide*, Reichhold, Inc., Research Triangle Park, NC 27709. 2009.
151. a) N.L. Newhouse, G.B. Rawls, M.D. Rana, B.F. Shelley, M.R. Gorman, "Development of ASME section X code rules for high pressure composite hydrogen pressure vessels with non-load sharing liners", Proceedings of the 2010 ASME Pressure Vessels and Piping Conference, PVP 2010, Paper No. PVP2010-25349, 2010, 10 p.
b) ASME Boiler and Pressure Vessel Code, Sec. X, Fiber-reinforced Plastic Pressure Vessels, Mandatory Appendix 8-620 and NB10-0601, Supplement 9.
152. M.R. Gorman, "Modal AE analysis of fracture and failure in composite materials, and the quality and life of high pressure composite pressure vessels", J. Acoustic Emission, vol. 29, 2011, pp. 1-28.
153. C.C. Ciang, J.R. Lee and H.J. Bang, "Structural health monitoring for a wind turbine system: a review of damage detection methods", Meas. Sci. Technol. vol. 19, 2008, 122001 (20 pp) doi:10.1088/0957-0233/19/12/122001
154. B. Lu, Y. Li, X. Wu and Z. Yang, "A review of recent advances in wind turbine condition monitoring and fault diagnosis", *Proc. IEEE conference on power electronics and machines in wind applications*. 2009. pp. 1-7.
155. M A Drewry and G A Georgiou, "A review of NDT techniques for wind turbines", Insight, vol. 49 no. 3 March 2007, pp. 137-141. www.ndt.net/search/docs.php3?id=4550
156. K.K. Borum, M. McGugan and P. Brøndsted, "Condition monitoring of wind turbine blades", *Polymer Composite Materials for Wind Power Turbines*, eds: H. Lilholt et al., Risø National Laboratory, Roskilde, Denmark, 2006, pp. 139-145.
157. M.A. Rumsey, J. Paquette, J.R. White, R.J. Werlink, A.G. Beattie, C.W. Pitchford, J. van Dam, "Experimental Results of Structural Health Monitoring of Wind Turbine Blades", AIAA paper AIAA-2008-1348, 2008. sandia.gov/wind/asme/AIAA-2008-1348.pdf
158. A.A. Anastassopoulos, D.A. Kouroussis, V.N. Nikolaidis, A. Proust, A.G. Dutton, M.J.

Blanch, L.E. Jones, P. Vionis, D.J. Lekou, D.R.V. van Delft, P.A. Joosse, T.P. Philippidis, T. Kossivas, G. Fernando, "Structural integrity evaluation of wind turbine blades using pattern recognition analysis on acoustic emission data", EWGAE22, vol. I, 2002, pp. 21-28.
159. P.A. Joosse, M.J. Blanch, A.G. Dutton, D.A. Kouroussis, T.P. Philippidis, P. Vionis, "Acoustic emission monitoring of small wind turbine blades", *Proc. 21st ASME Wind Energy Symp*., 2002, AIAA-2002-0063 pp. 1–11.
160. G.R. Kirikera, V. Shinde, M.J. Schulz, A. Ghoshal, M. Sundaresan and R. Allemang, 2007 "Damage localization in composite and metallic structures using a structural neural system and simulated acoustic emissions", Mech. Syst. Signal Process. vol. 21, 2007, pp. 280–297.
161. W. Prosser, E. Madaras, G. Studor, and M. Gorman, "Acoustic emission detection of impact damage on space shuttle structures", J. Acoustic Emission. vol. 23, 2005, pp. 37-46.
162. W. Prosser, E. Madaras, G. Studor, and M. Gorman, "Thermal protection system monitoring of space structures", *Encyclopedia of Structural Health Monitoring*, eds. C. Boller et al., J. Wiley, 2009, pp. 289-298.
163. A. Marshall, "Sandwich construction", Handbook of Composites, ed. G. Lubin, Van Nostrand Reinhold, 1982, pp. 557-601.
164. M. Burman, "Fatigue crack initiation and propagation in sandwich structures", PhD thesis, Department of Aeronautics, Kungliga Tekniska Högskolan, (Royal Institute of Technology), S-100 44 Stockholm, Sweden, Report No. 98-29, 1998, 171 p.
165. R.E. Rodriguez-Vera, N.J. Lombardi, M.A.S. Machado, J. Liu, E.D. Sotelino, "Fiber reinforced polymer bridge decks", FHWA/IN/JTRP-2011/04, 2011, Purdue Univ., W. Lafayette, IN, 99 p.
166. J.C. Flannigan, "Acoustic emission monitoring on fiber reinforced bridge panels", MS thesis, Kansas State University, Manhattan, Kansas, 2008, 68 p.
167. P. Ouellette and S.V. Hoa, "Acoustic emission signal trends during high cycle fatigue of FRP/balsa wood core vessels", J. Acoustic Emission. vol. 11, no. 2, 1993, pp. 65-70.
168. H. Pfeiffer, M. Wevers, "Aircraft integrated structural health assessment – structural health monitoring and its implementation within the European project AISHA", EU Project Meeting on Aircraft Integrated Structural Health Assessment (AISHA), Leuven, Belgium, June 2007. www.ndt.net/search/docs.php3?MainSource=69
169. N. Takeda and S. Minakuchi, "Recent development of structural health monitoring technologies for aircraft composite structures in Japan", Proc. 17th Int. Conf. on Composite Materials (ICCM-17), Edinburgh, UK, 27-31 July 2009.
170. G. Tober, D. Schiller, "NDT in aerospace - state of art", WCNDT paper, 2000.
http://www.ndt.net/article/wcndt00/papers/idn904/idn904.htm
171. H. Speckmann, R. Henrich, "Structural Health Monitoring (SHM) - Overview on Airbus activities", Proc. 16th World Conf. NDT, Montreal 2004, paper 536.
172. U. Schnars, R. Henrich, "Applications of NDT methods on composite structures in aerospace industry", Online-Proc. Conf. on Damage in Composite Materials – CDCM2006, vol. 12, no. 12 (2006). http://www.ndt.net/article/cdcm2006/
173. D. Roach, Assessing conventional and advanced NDI for composite aircraft", High Performance Composites, June 2008, 3 p. http://www.compositesworld.com/articles/assessing-conventional-and-advanced-ndi-for-composite-aircraft
174. a) T. Ullmann, T. Schmidt, S. Hofmann, R. Jemmali, "In-line quality assurance for the manufacturing of carbon fiber reinforced aircraft structures", *2nd Intl Symp. on NDT in Aerospace 2010* - Tu.1.A.4. http://www.ndt.net/article/aero2010/papers/tu1a4.pdf
b) V. Giurgiutiu, A. Zagrai, J.J. Bao, J.M. Redmond, D. Roach, K. Rackow, "Active sensors for health monitoring of aging aerospace structures", Intl J. of COMADEM, vol. 6(1) January 2003, pp. 3-21.

175. B.C. Dykes and W.T. Hardrath, “An acoustic emission pre-failure warning system for composite structural tests”, ref. 24d, 1992, pp. 175-180.
176. D. Lindahl and M. Knuuttila, “Acoustic emission monitoring of the Jas 39 Gripen Combat Aircraft”, *Progress in AE, X*, (IAES15), Japanese Society for NDI, 2000, pp. 219-224.
177. F.A. Leone, Jr., D. Ozevin, V. Godinez, B. Mosinyi, J.G. Bakuckas, Jr., J. Awerbuch, A. Lau, T.-M. Tan, “Acoustic emission analysis of full-scale honeycomb sandwich composite curved fuselage panels”, *Proc. of SPIE*, vol. 6934, 2008, pp. 1-16.
178. D. Aljets, “*Acoustic Emission Source Location in Composite Aircraft Structures using Modal Analysis*”, Ph.D. Thesis, Faculty of Advanced Technology, University of Glamorgan, June 2011, 163 p. http://dspace1.isd.glam.ac.uk/dspace/bitstream/10265/575/1/PhD%20Thesis%20Dirk%20Aljets.pdf
179. D. Aljets, A. Chong, S. Wilcox, K. Holford, “Acoustic emission source location in plate-like structures using a closely arranged triangular sensor array” J. Acoustic Emission, vol. 28, 2011, pp. 85-98.
180. W.H. Sachse, S. Sancar, “Acoustic emission source location on plate-like structures using a small array of transducers”, US Patent 4,592,034, May 27, 1986.
181. C.M. Yeum, H. Sohn, J.B. Ihn, “Lamb wave mode decomposition using concentric ring and circular piezoelectric transducers”, Wave Motion, vol. 48, 2011, pp. 358–370.
182. M. Wevers, L. Rippert, and S. Van Huffel, “Optical fibres for in situ monitoring the damage development in composites and the relation with acoustic emission measurements”, J. Acoustic Emission. vol. 18, 2000, pp. 41-50.
183. M. Surgeon, M. Wevers, “The influence of embedded optical fibres on the fatigue damage progress in quasi-isotropic CFRP laminates”, J. Composite Materials, vol. 35, 2001, pp. 931-940.
184. S. Vandenplas, J.-M. Papy, M. Wevers, S. Van Huffel and D. Inaudi, “Acoustic emission monitoring using a polarimetric single mode optical fiber sensor”, Proc. SPIE 5855, 17th Intl. Conf. on Optical Fiber Sensors, 2005, p. 1064.
185. M. Wevers, L. Rippert, J.-M. Papy, and S. Van Huffel, “Processing of transient signals from damage in CFRP composite materials monitored with embedded intensity-modulated fiber optic sensors”, NDT&E Int., vol. 39, 2006, pp. 229-235,
186. I. Ohsawa, K. Kageyama, Y. Tsuchida, M. Kanai, “Development of a novel optical fiber sensor for AE detection in composites”, J. Acoustic Emission. vol. 21, 2003, pp. 176-186.
187. H. Cho, R. Arai, M. Takemoto, “Development of stabilized and high sensitive optical fiber acoustic emission system and its application”, J. Acoustic Emission, vol. 23, 2005, pp. 72-80.
188. T. Matsuo, H. Cho, M. Takemoto, “Utilization of cascade optical fiber ae system for source location of Lamb waves through a cross-ply CFRP plate”, J. Acoustic Emission. vol. 24, 2006, pp. 84-96.
189. H. Tsuda, “A Bragg wavelength-insensitive fiber Bragg grating ultrasound sensing system that uses a broadband light and no optical filter”, Sensors, vol. 11, 2011, pp. 6954-6966.
190. P.M. Lam, K.T. Lau, H.Y. Ling, Z.Q. Su, H.Y. Tam, “Acousto-ultrasonic sensing for delaminated GFRP composites using an embedded FBG sensor" Opt. Laser Eng. vol. 47, 2009, pp. 1049-1055.
191. M. Ohtsu and K. Ono, "Pattern Recognition Analysis of Magneto mechanical Acoustic Emission Signals," J. Acoustic Emission, vol. 3(2), 1984, pp. 69-80.
192. K. Ono, K. Kawamoto, "Digital signal analysis of acoustic emission from carbon fiber/epoxy composites," J. Acoustic Emission, vol. 9, 1990, pp. 109-116.
193. A.A. Anastassopoulos and T.P. Philippidis, Clustering methodology for the evaluation of acoustic emission from composites”, J. Acoustic Emission, vol. 13, 1995, pp. 11-22.

194. E.v.K. Hill, S.-A.T. Dion, J.O. Karl, N.S. Spivey and J.L. Walker II, "Neural network burst pressure prediction in composite overwrapped pressure vessels," J. Acoustic Emission, vol. 25, 2008, pp. 187-193.
195. F.F. Barsoum, J. Suleman, A. Korcak E.v.K. Hill, "Acoustic emission monitoring and fatigue life prediction in axially loaded notched steel specimens," J. Acoustic Emission, vol. 27, 2009, pp. 40-63.
196. T. Kohonen, "The self-organizing map", *Proc. IEEE*, vol. 78, no. 9, 1990, pp. 1464-1480.
197. V. Emamian, M. Kaveh, and A.H. Tewfik, "Robust clustering of acoustic emission signals using the Kohonen network," in *Proc. IEEE Int. Conf. Acoustics, Speech, Signal Processing*, vol. 6, Istanbul, Turkey, June 2000, pp. 3891–3894.
198. M.L. Marsden and E.v.K. Hill, "Classification of Fatigue Cracking Data in a Simulated Aircraft Fuselage Using a Self Organizing Map," *First International Conference on Nonlinear Problems in Aviation and Aerospace,* S. Sivasundaram, editor, Embry-Riddle Aeronautical University Press, Daytona Beach, FL, 1997, pp. 405-410.
199. E.v.K. Hill, J. Iizuka, I.K. Kaba, H.L. Surber, Y.P. Poon, "Neural network burst pressure prediction in composite overwrapped pressure vessels using mathematically modeled acoustic emission failure mechanism data", Research in Nondestructive Evaluation, vol. 23, 2012, pp. 89–103.
200. R. Gutkin, C.J. Green, S. Vangrattanachai, S.T. Pinho, P. Robinson, P.T. Curtis, "On acoustic emission for failure investigation in CFRP: Pattern recognition and peak frequency analyses", Mechanical Systems and Signal Processing, vol. 25, 2011, pp. 1393-1407.
201. R. de Oliveira, A.T. Marques, "Health monitoring of FRP using acoustic emission and artificial neural networks", Computers and Structures, vol. 86, 2008, pp. 367–373.

Appendix 1: Lamb wave propagation

In 1986, Ichikawa et al. [A1] investigated the optimum conditions for using Lamb waves for inspection of steel sheets, which fail from nonmetallic inclusions under heavy deformation. Using theoretical results, they developed an improved inspection system for use in steel production lines. From the basic Lamb wave behavior, they noted complexity, such as 1) some modes are difficult to excite or detect depending on frequency-thickness product, or $f{\cdot}d$ values, 2) the sharpness of flaw reflection varies strongly with $f{\cdot}d$ values, and 3) flaw reflection pulse has a different frequency from that of the excitation pulse.

Pulse excitation and detection typically uses piezoelectric sensors that respond to normal displacement; on the plate surfaces, one needs vertical particle displacements from Lamb waves. For a plate of thickness, d, scalar and vector potentials are introduced to represent displacement and stress within the plate using free boundary conditions on the surfaces. The components of a displacement vector (U, W) for the wave propagation direction, x, and for the normal (thickness) direction, z, are given by:

For symmetric modes:

$$\left.\begin{aligned} U &= \alpha k_s \left(\frac{\cosh q_s z}{\sinh q_s \delta} - \frac{2 q_s s_s}{k_s^2 + s_s^2} \times \frac{\cosh s_s z}{\sinh s_s \delta} \right) \\ &\quad \times \exp\left[i\left(k_s x - \omega t - \frac{\pi}{2} \right) \right] \\ W &= -\alpha q_s \left(\frac{\sinh q_s z}{\sinh q_s \delta} - \frac{2 k_s^2}{k_s^2 + s_s^2} \times \frac{\sinh s_s z}{\sinh s_s \delta} \right) \\ &\quad \times \exp[i(k_s x - \omega t)] \end{aligned}\right\} \quad (3a)$$

For asymmetric modes

$$\left.\begin{aligned} U &= \beta k_a \left(\frac{\sinh q_a z}{\cosh q_a \delta} - \frac{2 q_a s_a}{k_a^2 + s_a^2} \times \frac{\sinh s_a z}{\cosh s_a \delta} \right) \\ &\quad \times \exp\left[i\left(k_a x - \omega t - \frac{\pi}{2} \right) \right] \\ W &= -\beta q_a \left(\frac{\cosh q_a z}{\cosh q_a \delta} - \frac{2 k_a^2}{k_a^2 + s_a^2} \times \frac{\cosh s_a z}{\cosh s_a \delta} \right) \\ &\quad \times \exp[i(k_a x - \omega t)] \end{aligned}\right\} \quad (3b)$$

where $d = 2\delta$, $q_s^2 = k_s^2 - k_l^2, q_a^2 = k_a^2 - k_l^2, s_s^2 = k_s^2 - k_t^2, s_a^2 = k_a^2 - k_t^2$, $\omega = 2\pi f$: angular frequency, $k_{s\,(a,\,l,\,t)}$: wave number for symmetric (asymmetric, longitudinal, transverse) wave, α, β = constant. W_δ is defined as an index to express the magnitude of the surface normal displacement, W, relative to the integrated mean-square displacement as:

$$W_\delta = \frac{[W]_{z=\delta}}{\sqrt{\int_{-\delta}^{\delta} (U^2 + W^2)\,dz}} \quad (4)$$

Using equations 3 and 4 with the shear modulus of steel = 80.3 GPa, density = 7.8 Mg/m^3, Poisson's ratio = 0.28, the phase velocity and W_δ in dB scale are shown against $f{\cdot}d$ in Fig. A1 (a) and (b). These are reproduced from Figs. 4 and 5 in [A1]. It is evident that W_δ varies widely depending on the wave mode and $f{\cdot}d$ values. It is significant that the surface normal displacement

of S_o mode is less than –17 dB for $f \cdot d \leq 1$ MHz·mm, while that for A_o is always above –6 dB. This explains why S_o mode is usually not observed at low frequencies, especially for thin structures.

The wave dispersion also affects the pulse amplitude. The group velocity C_g is given by

$$\frac{C}{C_g} = 1 - \frac{f}{C}\left(\frac{\partial C}{\partial f}\right), \tag{5}$$

where C is the phase velocity. When a pulse with the center frequency f_o and its spread in the frequency domain Δf (in half-value width) travels time t over distance l, resulting in pulse spread in time of Δt (in half-value pulse width) of:

$$\begin{aligned} \Delta t &= A_0\left[\frac{\partial t}{\partial f}\right]_{f=f_0} \times \Delta f \\ &= A_0 l \Delta f\left[\frac{\partial C_g}{\partial f}\Big/ C_g^2\right]_{f=f_0} \end{aligned} \tag{6}$$

where A_o is a constant. A parameter D_g defined below indicates the sharpness of a pulse affected by the velocity dispersion. With the transverse velocity C_t, we have:

$$D_g = \frac{\partial}{\partial(fd)}\left(\frac{C_g}{C_t}\right)\Big/\left(\frac{C_g}{C_t}\right)^2 \tag{7}$$

Results of calculation are shown in Fig. A1(c) (which is Fig. 6 in [A1]). When the value of D_g vanishes, the dispersion effect is minimal. Again, D_g varies strongly with $f \cdot d$ values, depending on the wave mode. Open circles marked P_1 to P_8 (in Fig. A1 (b) and (c)) indicate the points where $D_g = 0$. Table 1 in [A1] gives the $f \cdot d$ values (along with C/C_L, C_g/C_L and W_d (in dB)) corresponding to P_1 to P_8 :

P_i	P_1	P_2	P_3	P_4	P_5	P_6	P_7	P_8
$f \cdot d$ value	1.42	2.52	2.80	4.81	6.97	7.26	7.41	9.09
wave mode	A_o	S_o	A_1	A_1	S_1	A_3	A_3	A_2
C/C_L	0.79	1.23	2.00	1.33	1.38	2.80	2.60	1.40
C_g/C_L	1.01	0.54	1.18	0.69	0.70	0.78	0.78	0.71
W_d (in dB)	-6.0	-4.0	-8.5	-5.1	-5.2	-3.8	-3.9	-5.1

There seems another vanishing D_g point at $f \cdot d = 4.12$ for S_1 mode, but W_δ is low here. Judging from various wave propagation data, both theoretical and experimental, it appears that when $D_g \leq \pm 0.3 \sim 0.5$, pulse propagation is possible without suffering excessive dispersion effects.

Considering both W_δ and D_g, this work leads to approximate ranges where good pulse detection with low dispersion loss can be expected:

S_o mode	$f \cdot d = 1 \sim 2, > 3.5$
A_o mode	> 0.5
S_1 mode	~ 2.7
A_1 mode	$2 \sim 4$
S_2 mode	$3.5 \sim 7$
A_2 mode	> 5.8

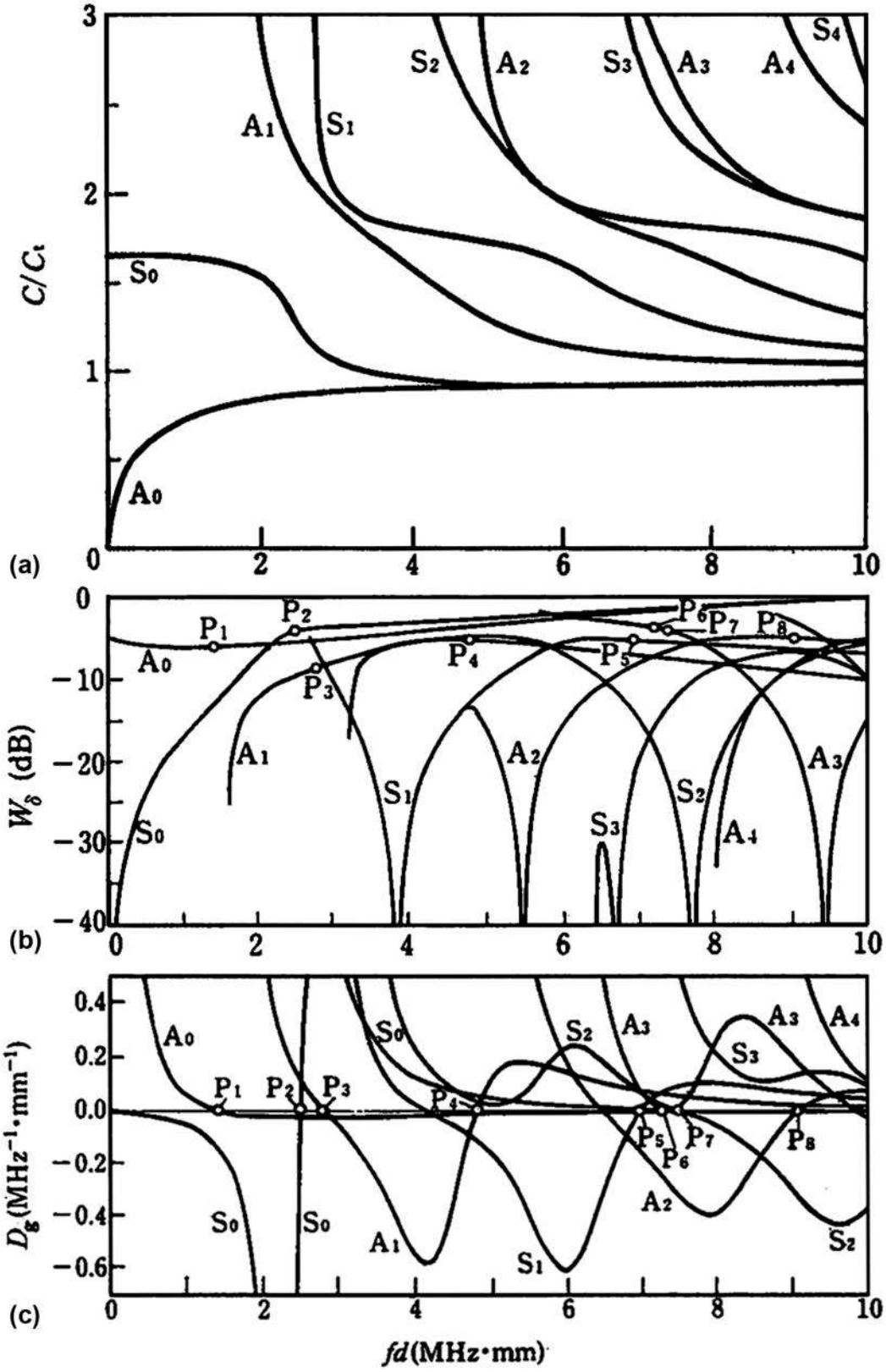

Fig. A1. a) Phase velocity of Lamb waves vs. $f{\cdot}d$ values. b) Index for surface normal displacement W_δ in dB scale vs. $f{\cdot}d$ values. c) Parameter for dispersion effect D_g vs. $f{\cdot}d$ values. These figures were assembled from Figs. 4-6 in Ichikawa et al. [A1], matching the abscissa.

Since W_δ is in dB scale, it should dictate the outcome, while effects of D_g parameter needs to be explored experimentally.

This result of Ichikawa et al. [A1] is for isotropic medium and not directly applicable to fiber composite materials. However, this gives for the first time explanations for oft-peculiar Lamb-wave propagation behavior. In practical inspection setups, one also needs to consider frequency-dependent attenuation effects.

Appendix 2: Gaussian Pulses

A Gaussian pulse is defined as a function of time *t*

$$G(t) = \exp[-t^2/2\sigma^2] \quad (8)$$

where σ is a pulse width parameter [A2]. The pulse width at one-half of the peak height, $t_{1/2}$, (also called the full width at half-maximum or FWHM) is given by

$$t_{1/2} = \sqrt{8 \ln (8)}\, \sigma = 2.35482\, \sigma. \quad (9)$$

Figure A2 (a) shows a Gaussian pulse with $t_{1/2}$ = 0.22 μs [A3]. The power spectral density of this pulse is given in Fig. A2 (b). It peaks at f = 0 and the spectral width at one-half of the peak height, $f_{1/2}$, is equal to 2.0 MHz. The half-height widths are related to each other by [A4]

$$t_{1/2} \text{ x } f_{1/2} = 0.44. \quad (10)$$

The time derivative of a Gaussian pulse defines a Gaussian mono-pulse (aka monocycle). Using the center frequency, f_c, it is given by [A5]

$$V(t, f_c, A) = 2\sqrt{e}\, A\pi t\, f_c \exp[-2(\pi t f_c)^2], \quad (11)$$

where *A* is the peak height. A Gaussian mono-pulse at 2 MHz is shown in Fig. A2 (c) [A6]. In the frequency domain, this is given by

$$V(f, f_c, A) = \frac{A}{2}\sqrt{\frac{2e}{\pi}}\frac{f}{f_c} \exp\left[-\frac{1}{2}\left(\frac{f}{f_c}\right)^2\right]. \quad (12)$$

The inverse of the center frequency is essentially pulse duration, τ. That is,

$$\tau \text{ x } f_c \sim 1. \quad (13)$$

A pair of waveform and its frequency spectrum from [A5] was scaled to 2 MHz to 200 kHz center frequencies. Four such pairs are illustrated in Fig. A3, (a) to (d).

The most striking feature of Fig. A3 is the broadness of the spectra. For a 2 MHz pulse (of 0.5-μs duration), –3 dB half-power points are at 1 and 3.2 MHz. At 200 kHz (5-μs long pulse), the corresponding frequency range is from 100 to 320 kHz. Thus, a variation in source duration has to be quite large to be noticeable in the detected frequency spectra. Since most sensors and structures have natural frequencies, their dominance will be difficult to overcome.

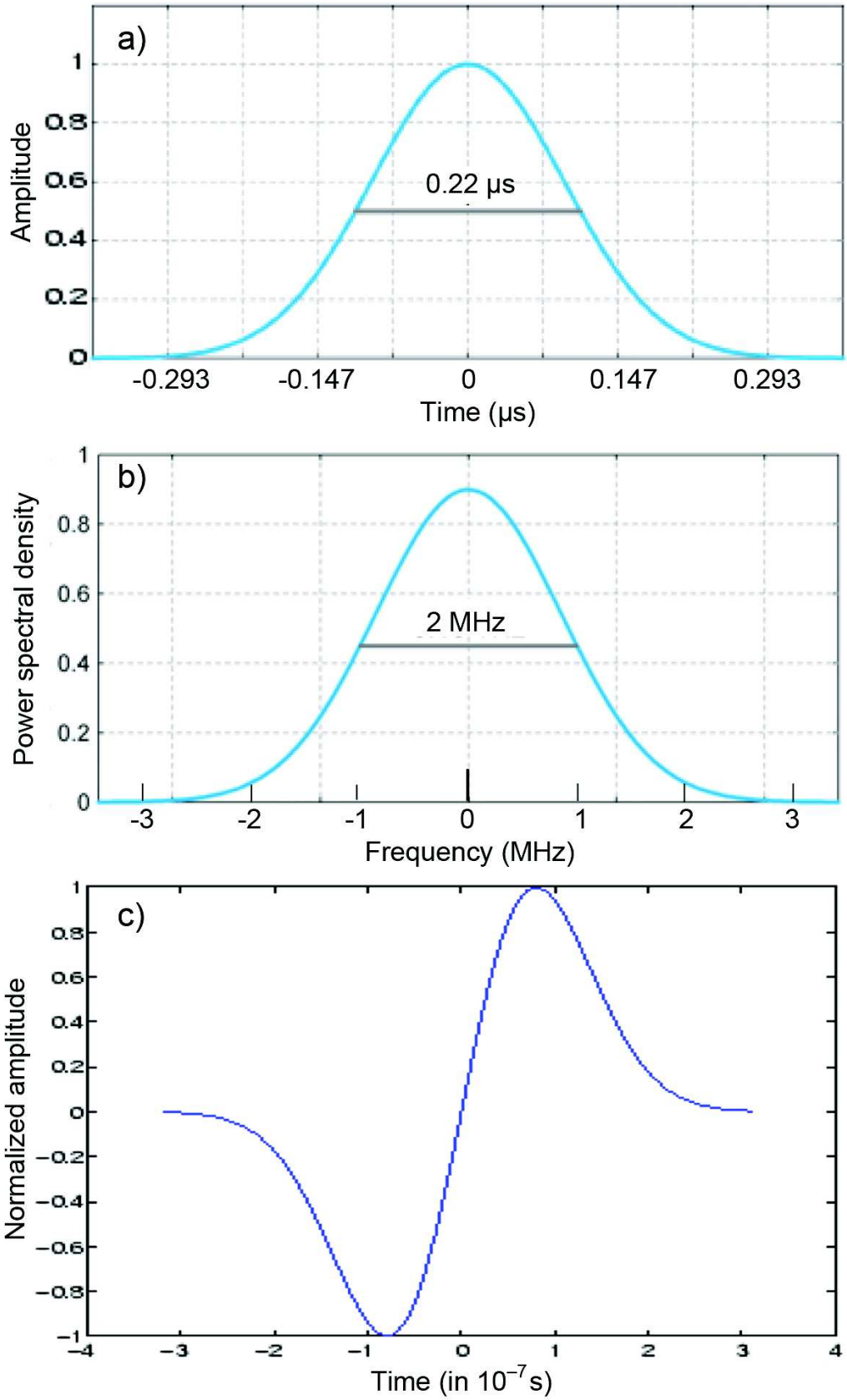

Fig. A2. a) 2-MHz Gaussian pulse. b) Its power spectral density. [A3] c) 2-MHz Gaussian mono-pulse. [A6]

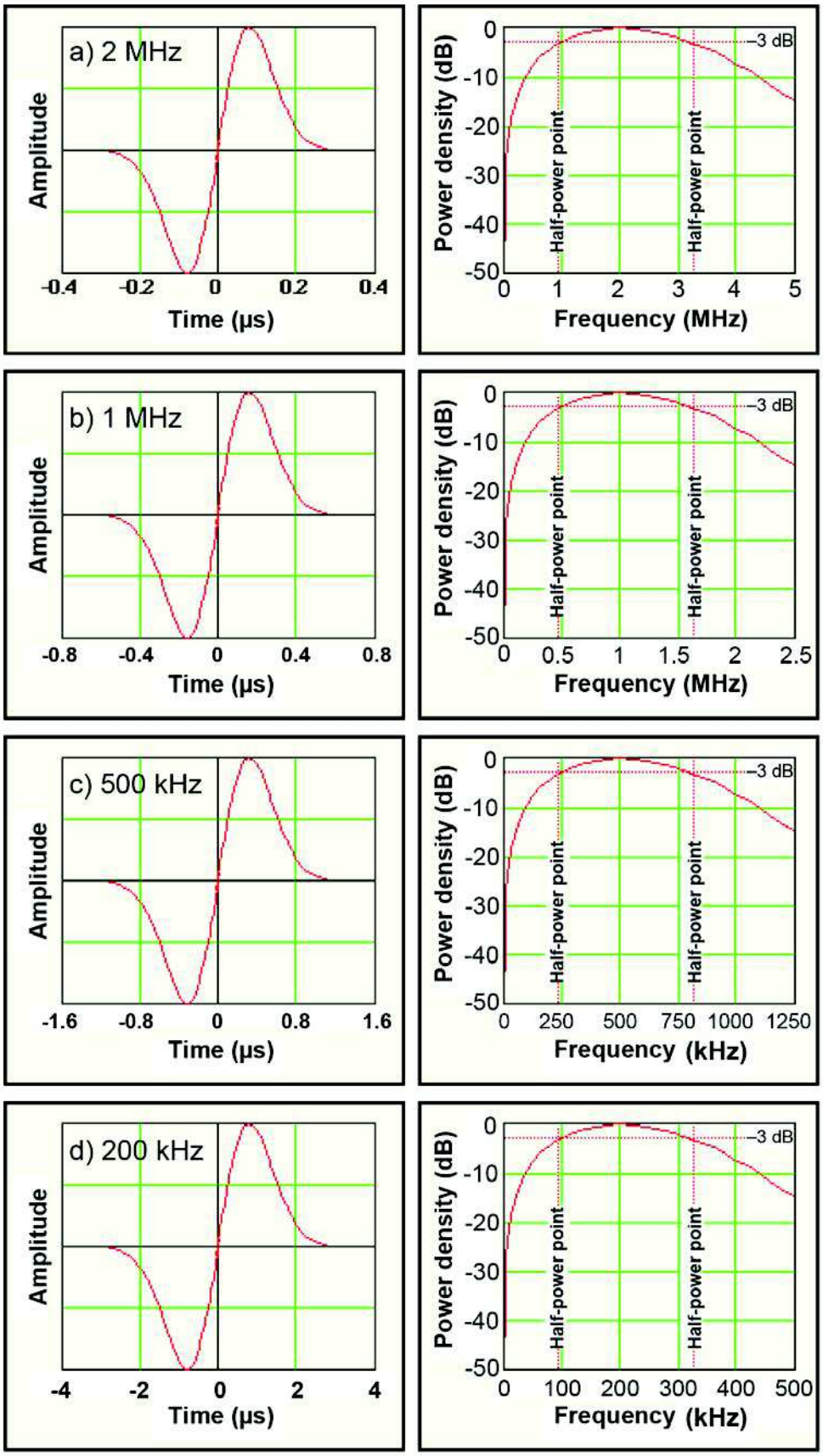

Fig. A3. a) 2-MHz Gaussian monopulse and its power spectral density. b) Same for 1 MHz. c) Same for 500 kHz. d) Same for 200 kHz. [A5]

Appendix 3: Directionality of Attenuation and Source Types

Suzuki [71b] measured P-wave attenuation in UD-GFRP with 60% fiber content using a laser technique. Figures 4.15(g), 4.16 and 4.17 from his thesis are shown in Fig. A4 below. These show high attenuation especially for 90º orientation at 160-180 dB/m, but even for the orientation along fibers (0º) it is 60~80 dB/m. These are still 2 to 5 times less than in epoxy.

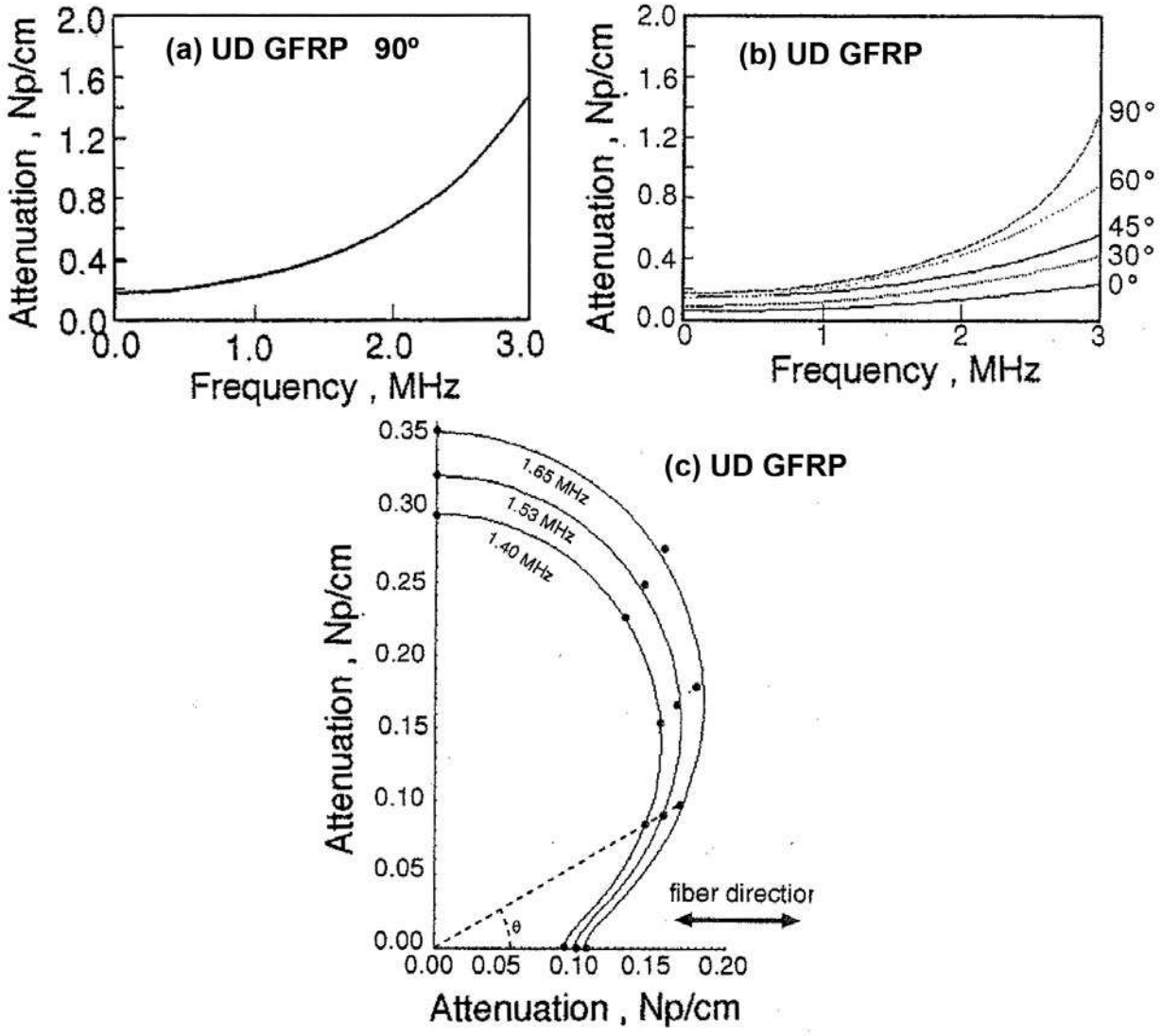

Fig. A4. a), b) Frequency dependence of P-wave attenuation in GFRP. c) Orientation dependence at 1.4~1.65 MHz. [71b]

Downs et al. [A7] examined the directionality of AE sources in an Al plate, that is, the orientation dependence of FEM-generated AE signals due to three types of sources, i.e., in-plane dipole, microcrack initiation, and shear at 45° about the y-axis without a moment. They used wavelet transform to characterize the absolute WT peak magnitude as a function of radiation angle and source depth. The fall-off with increasing angle is dramatic for the in-plane dipole (nearly 100 %), as shown in Fig. A5. It is least for the microcrack initiation, except for a source at the mid-plane, where the 45° shear has the least fall-off. The results also demonstrated that the WT absolute peak magnitudes have their greatest values when the source is close to the surface and have their lowest values when the source is located at or near the mid-plane.

The directionality WT magnitude of microcrack sources is shown in Fig. A6, where 0º-amplitude was used to normalize other radiation angles. Here, frequency: 270 kHz, propagation distance: 180 mm, plate thickness: 4.7 mm. S_0 and A_0 data behaved differently; Source depth effect was present for the A_0 mode, but not for the S_0 mode. In both modes, the magnitude did not vanish at 90º.

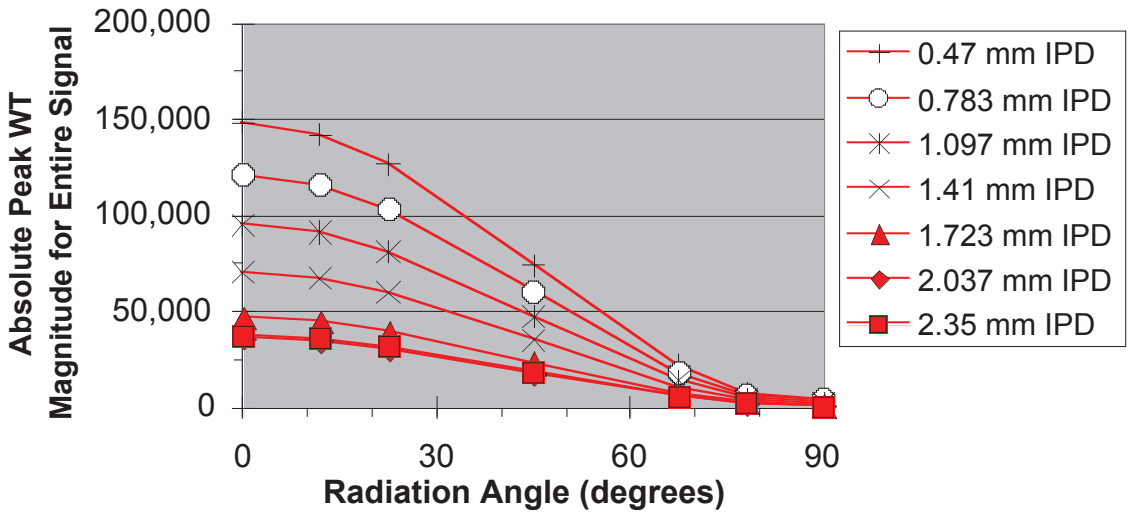

Fig. A5. Absolute peak WT magnitudes for various source depths for in-plane dipole source at 180 mm propagation distance [A7].

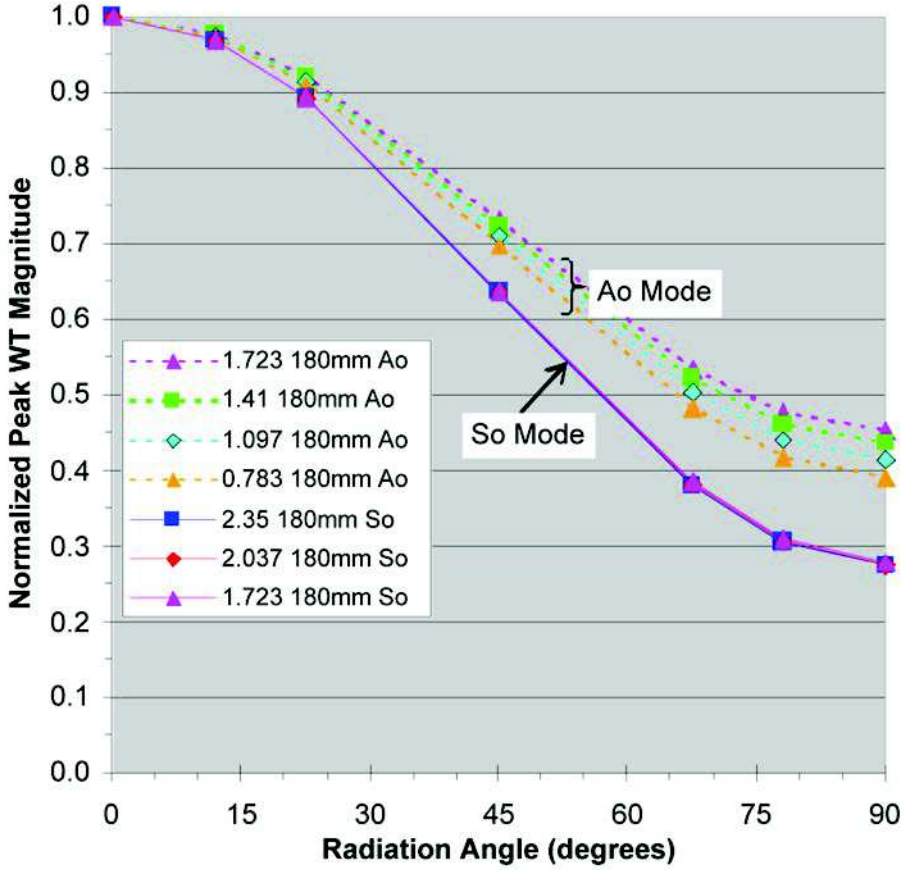

Fig. A6. Normalized peak WT magnitudes for microcrack source at 270 kHz; legend lists source depth (mm), propagation distance (mm), and mode [A7].

References for Appendices

A1. F. Ichikawa, K. Kurita, H. Maruyama, S. Takahashi, "Study on optimum conditions for Lamb wave ultrasonic testing and its application to product line", Kawasaki Steel Tech. Report, vol. 18, 1986, pp. 192-198.

A2. S. Smith, Gaussian Pulses. http://gamma.ethz.ch/download/pdf/pulses/gaussian.pdf

A3. Introduction to Optical Pulses, Optipedia, Free optics information SPIE. Excerpt from R. Paschotta, Field Guide to Laser Pulse Generation, SPIE Press, Bellingham, WA (2008). spie/org/x32442/xml?pf=true

A4. Gaussian pulses, Encyclopedia of Laser Physics and Technology. www.rp-photonics.com/gaussian_pulses.html

A5. P. Withington, Impulse Radio Overview, Time Domain Corp. user.it.uu.se/~carle/Notes/UWB.pdf

A6. Gaussian monopulse – Matlab: www.mathworks.com/help/toolbox/signal/ref/gmonopuls.html

A7. K.S. Downs, M.A. Hamstad and A. O'Gallagher, "Practical aspects of acoustic emission source location by a wavelet transform", J. Acoustic Emission, vol. 21, 2003, pp. 52-69.